14

Magnonic Metamaterials

V.V. Kruglyak et al.*
School of Physics,
University of Exeter, Exeter,
United Kingdom

1. Introduction

A large proportion of the recent growth of the volume of electromagnetics research has been associated with the emergence of so called electromagnetic metamaterials[1] and the discovered ability to design their unusual properties[2,3] by tweaking the geometry and structure of the constituent "meta-atoms"[4]. For example, negative permittivity and negative permeability can be achieved, leading to negative refractive index metamaterials[2]. The negative permeability could be obtained via geometrical control of high frequency currents, e.g. in arrays of split ring resonators[5], or alternatively one could rely on spin resonances in natural magnetic materials[6,7], as was suggested by Veselago in Ref. 2. The age of nanotechnology therefore sets an intriguing quest for additional benefits to be gained by structuring natural magnetic materials into so called *magnonic* metamaterials, in which the frequency and strength of resonances based on spin waves (magnons)[8] are determined by the geometry and magnetization configuration of meta-atoms. Spin waves can have frequencies of up to hundreds of GHz (in the exchange dominated regime)[6-9] and have already been shown to play an important role in the high frequency magnetic response of composites[10-14]. Moreover, in view of the rapid advances in the field of magnonics[9,15,16,], which in particular promises devices employing propagating spin waves, the appropriate design of magnonic metamaterials with properties defined with respect to propagating spin waves rather than electromagnetic waves acquires an independent and significant importance.

*M. Dvornik[1], R.V. Mikhaylovskiy[1], O. Dmytriiev[1], G. Gubbiotti[2,3], S. Tacchi[3], M. Madami[3], G. Carlotti[3], F. Montoncello[4], L. Giovannini[4], R. Zivieri[4], J.W. Klos[5], M.L. Sokolovskyy[5], S. Mamica[5], M. Krawczyk[5], M. Okuda[6], J.C. Eloi[6], S. Ward Jones[6], W. Schwarzacher[6], T. Schwarze[7], F. Brandl[7], D. Grundler[7], D.V. Berkov[8], E. Semenova[8] and N. Gorn[8]
[2]*Istituto Officina dei Materiali del Consiglio Nazionale delle Ricerche (IOM-CNR), Sede di Perugia, c/o Dipartimento di Fisica, Perugia, Italy*
[3]*CNISM, Unità di Perugia and Dipartimento di Fisica, Perugia, Italy*
[4]*Dipartimento di Fisica and CNISM, Università di Ferrara, Ferrara, Italy*
[5]*Faculty of Physics, Adam Mickiewicz University, Poznan, Poland*
[6] *H. H. Wills Physics Laboratory, Bristol, United Kingdom*
[7]*Lehrstuhl fuer Physik funktionaler Schichtsysteme, Physik Department, Technische Universität München, Garching bei Muenchen, Germany*
[8]*Innovent Technology Development, Jena, Germany*

In this Chapter, we review the recent advances in studies of magnonic metamaterials and challenges that have to be overcome in order for the rich opportunities of exploitation of such metamaterials to be realised. We start from a discussion of the notion of a metamaterial and its relevance to areas beyond that of common electromagnetics. We introduce band gap and effectively continuous magnonic metamaterials and demonstrate their properties and functionalities, presenting either experimental or theoretical evidence as appropriate for the illustration.

2. What makes a metamaterial?

To answer the question in the title in the most general sense (i.e. going beyond the topic of more common electromagnetic metamaterials), one has to learn first what makes standard (i.e., "nature-made") *materials*. One talks about a material when many atoms or ions are joined together to collectively create a novel quality with properties that are not observed in the constituent atoms in isolation. For example, isolated atoms have discrete electronic energy levels and associated discrete electromagnetic spectra. In a material consisting of many of such atoms, each discrete electronic level is split into a continuous "electronic band", and accordingly the electromagnetic spectrum of the material is also continuous.

As a result of joining into a material, atoms also collectively acquire new properties that are less trivially connected with those of isolated atoms. Firstly, different classes of materials are formed, including e.g. dielectrics, semiconductors, or metals, ferro-, piezo-, or segneto-electrics, dia-, para-, antiferro- or ferro-magnets, superconductors, materials with a range of different mechanical properties, etc. Secondly, new classes of waves (excitations) and their quanta (so called quasi-particles) are observed, including plasmons, magnons, phonons, excitons etc. One can also distinguish many "hybrids" of the solid state quasi-particles among themselves as well as with photons, e.g. surface plasmon-polaritons, magneto-excitons etc.

A material does not have to have a periodic arrangement of atoms and can be amorphous or quasi-crystalline. The classification of materials and their properties often does not have strict boundaries, while the differences are often quantitative. For example, dielectrics and semiconductors are different only by the size of the band gap; the same material can be ferromagnetic below and paramagnetic above a certain temperature, etc. Some electronic energy levels can remain discrete, therefore retaining their atomistic character. Materials can also consist of rather complex building blocks, e.g. molecules, crystal unit cells (often consisting of many atoms or ions), or crystallites. The most complex nature-made (truly functional!) materials – biological tissues – consist of living cells composed of millions of atoms.

This brings us to the idea of a *metamaterial* – an artificial assembly of "man-made" building blocks with tailored properties. Living aside static properties and biological tissues, the most practical ways to "tailor" properties of the building blocks are via their geometrical shaping and compositional modulation. The former leads to confinement of solid state excitations (e.g. those listed above) and hence to formation of a discrete spectrum of the allowed modes. Brought sufficiently close together, the blocks can form a metamaterial with the discrete spectrum split into a band structure.

Some metamaterials (e.g. arrays of voids) are simpler to consider as created by geometrical modification of previously continuous materials. This however does not exclude their treatment as if they were constructed from building blocks considered above. Also, one has to note that, from the point of view of electromagnetic waves, vacuum is a continuous material in that important sense that it supports propagation of electromagnetic waves. Therefore, even arrays of entirely disconnected blocks are metamaterials for electromagnetic waves. This distinguishes electromagnetic waves from the other excitations.

Generally, various dynamical properties of metamaterials can be considered relative to excitations with wavelength either comparable to or much greater than the characteristic size of the building blocks. The former case is associated with studies of artificial "band gap crystals", e.g. photonic[17], plasmonic[18], phononic[19], and magnonic[20] crystals. The latter case allows one to study the metamaterials as some effectively continuous media. The physical object under study is nonetheless the same in both cases. For example, metamaterials with artificial periodic modulation of the refractive index with periodicity comparable to the wavelength of electromagnetic waves in the visible range are known as photonic band gap structures, using which it is possible to enable propagation of light in particular directions, to localize it in chosen channels or zones, or even to completely prohibit its propagation. In the microwave frequency range, the same structures would behave as effectively continuous materials.

In a particular frequency region of interest, the same metamaterials can behave differently with respect to excitations of different kinds, e.g. electromagnetic, sound or spin waves. Attractive opportunities arise from use of one excitation, with respect to which the sample behaves as a discrete structure (e. g. a band gap metamaterial), to design a resonance feature for another excitation, with respect to which the structure behaves as quasi-continuous metamaterial. For example, plasmonic resonances can be used to alter effective electromagnetic properties in THz to visible frequency range. Magnonic and LC resonances can be used for the same purpose in GHz-THz and GHz frequency ranges, respectively.

A thorough reader will probably find that, although term "metamaterial" emerged recently as a result of ever increasing pressure to spice up funding applications and publications in high profile journals, the underpinning research can be sometimes traced back to the middle or even beginning of the 20th century. Yet, one can also argue that it is the recent advances in nanofabrication and experimental tools that justify the boom by allowing researchers to revisit the established notions at reduced length scales and to apply results to modern technology.

3. Spin waves and effectively continuous magnonic metamaterials

The main reason for electrically neutral atoms to be able to interact with electromagnetic radiation is that they themselves possess electrical structure. Indeed, each atom consists of positively charged core and negatively charged electrons. The core and electrons are not rigidly coupled, and so, the atom can be electrically polarised by and thereby interact with an external electric field.

However, the electric charge is not the only property responsible for the interaction of atoms or materials with electromagnetic radiation. In particular, spins and associated magnetic

moments of elementary particles are responsible for their interaction with an external magnetic field. Being always electrically neutral, some atoms still have a net magnetic moment and hence are called "magnetic". Generally, electromagnetic field interacts with charges more strongly than with spins, and so, the associated resonance frequencies are weaker in spin resonance experiments. However, via the quantum mechanical Pauli Exclusion Principle, the electron spin governs the order in which the electronic bands are populated by electrons, and thereby strongly affects the electromagnetic spectrum. As the other side of the same phenomenon, the Pauli Exclusion Principle and electrostatic interaction result in the exchange interaction between spins and are therefore responsible for the ordering of spins observed in e.g. ferromagnetic materials. The perturbations of the magnetic ordering are called spin waves – the central object of magnonics and magnonic metamaterials.

Spin waves exhibit most of the properties inherent to waves of other origins, including the excitation and propagation[21,22,23], reflection and refraction[24,25,26,27,28,29], interference and diffraction[30,31,32,33,34,35], focusing and self-focusing[36,37,38,39,40,41], tunnelling[42,43], Doppler effect[44,45,46], and formation of spin-wave envelope solitons[47,48,49,50]. Spin-wave quantization due to the finite size effect was discovered in thin films[51,52] and more recently in laterally confined magnetic structures[53,54,55,56,57,58], with their effect upon the high frequency permeability and the observation of a negative permeability discussed in Refs. 7 and 59, respectively.

The possibility of using spin waves for the design of high frequency permeability follows already from their first direct observation in cavity ferromagnetic resonance (FMR) experiments[60]. In the latter measurements, the precession of magnetisation[60] is detected by measuring spectra of the absorption of microwaves in the cavity containing the magnetic sample under study. The spectra are determined by the density of states of spin waves that can resonantly couple to the microwave field. The very long wavelength of microwaves, as compared to the length scale of magnetic structures of interest, limits the application of the FMR technique to studies of magnonic modes with significant Fourier amplitude at nearly zero values of the wave vector[52]. However, this also mimics potential applications in which either the electromagnetic response of a magnonic device containing nano-structured functional magnetic elements is read out by the effectively uniform electromagnetic field, or the magnonic (meta-) material[61] is supposed to absorb the incident electromagnetic radiation. Continuous magnetic materials and arrays of non-interacting magnetic elements appear preferred for such applications near the frequency of the uniform FMR. However, more sophisticated micromagnetic engineering is required to push up the frequency of operation of such materials e.g. using the exchange field[62], which originates from the strongest of the magnetic interactions, rather than the uniform anisotropy or applied magnetic field. An example of using the concept can be found e.g. in Ref. 7 and is also illustrated in Figure 1.

The FMR is conventionally used to study magnetisation dynamics at frequencies up to about 100 GHz. At higher frequencies, the mismatch between the linear momentum of free space electromagnetic radiation (photon) and that of a magnon increasingly prohibits an efficient coupling. Therefore, higher frequencies require one to use different experimental and technical concepts by which to interrogate and measure e.g. THz magnons. Here, methods, known e.g. from plasmonics, might help to couple light to magnons. For example,

the attenuated total reflection technique has been successfully applied to studies of magnons in antiferromagnets[63]. However, this field of research is still at its infancy and is not reviewed here to any significant extent.

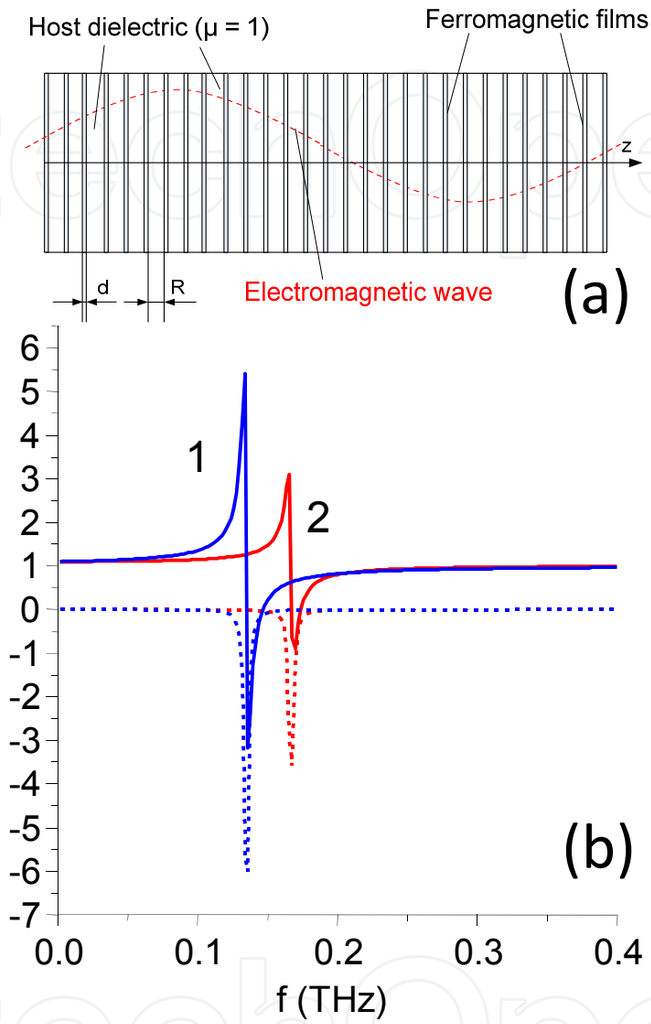

Fig. 1. (b) The effective permeability calculated for the structure shown in (a) is plotted as a function of the frequency for cases of in-plane (1) and out-of-plane (2) magnetizations. The solid and dashed lines denote the real and imaginary parts of the effective permeability, respectively. The structure under study represents an array of CoFe films with thickness of 5 nm. The filling factor of $\rho = 0.25$ is assumed. The spins are perfectly pinned at one side of each film and are free at the other. (After Ref. 7)

The VNA-FMR technique represents a relatively new twist in the FMR spectroscopy where VNA highlights the use of a broadband vector network analyser (VNA) operated in the GHz frequency regime. Microwaves applied to a waveguide locally excite spin waves that in turn induce a high-frequency voltage due to precessing magnetisation (Figure 2 (a)). The VNA-FMR technique measures spectra of both the amplitude and phase change of microwaves

passing through a magnetic sample integrated with the waveguide[64,65,66]. The geometrical parameters of the waveguide determine the spatial distribution of the rf magnetic field and therefore the wavelength spectrum addressed by the microwave field. Hence, the VNA-FMR can be also referred to as a "near field" FMR. Due to the large penetration depth of microwaves, both thin film and bulk samples can be successfully investigated using this technique.

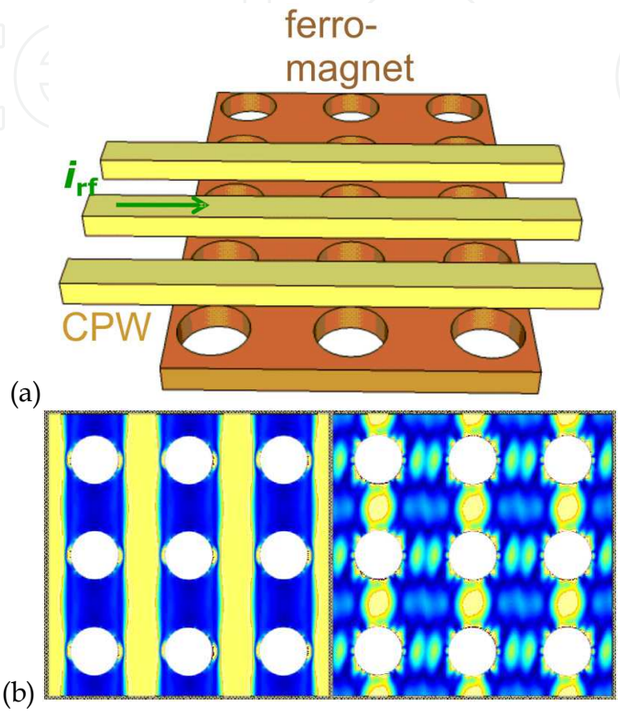

Fig. 2. (a) Sketch of a coplanar waveguide (CPW) integrated to an antidot lattice prepared from a thin Permalloy film. The CPW consists of three metallic leads (ground-signal-ground leads). Adjusting the dimensions of the CPW allows one to vary the profile of the magnetic field generated by microwave current i_{rf} supplied by the VNA. This defines the wave vector transferred to the sample. The same CPW picks up the voltage induced by precessing spins. The CPW is isolated from the ferromagnet by an insulating layer (not shown). (b) Simulated spatial distributions of spin precession amplitudes reflecting two different standing spin-wave excitations. The film is assumed to be 26 nm thick. The period (hole diameter) is 490 (240) nm. A magnetic field of a few 10 mT is applied in horizontal direction. The mode pattern shown on the right belongs to a localized mode that has frequency higher than that of the extended mode shown on the left. (After Ref. 91) Bright colours correspond to large amplitudes. The holes are shown in white.

An experimental insight into the structure of magnonic modes in nanostructured magnonic metamaterials, e.g. such those shown in Figure 2, can be achieved with state of art dynamic magnetic imaging techniques, e.g. the time-resolved scanning Kerr microscopy (TRSKM)[61]. In a TRSKM experiment, the sample is pumped so as to excite spin waves, with the pump stimulus being both repetitive and coherent, i.e. having a well-defined phase with respect to the probe beam. To probe, one uses ultrashort optical

pulses and controls their arrival time relative to the pump. By changing the optical path of the probe pulse one can trace the time evolution of the excited dynamics. By scanning the position of the optical probe on the surface of the sample, one acquires images of the dynamic magnetisation with a spatial resolution of down to 250 nm in real space[67-70], and is suitable for studying both continuous and nanostructured samples, as demonstrated in Figure 3. The temporal resolution of TRSKM can be well on the sub-ps time scale, therefore offering the detection of spin waves in the THz frequency regime. The TRSKM performs a 3D vectorial analysis of the time dependent magnetization[71] and is therefore phase sensitive. Alternatively, one can combine the magneto-optical detection with a VNA-FMR setup to image spin wave modes in the frequency rather than time domain[72].

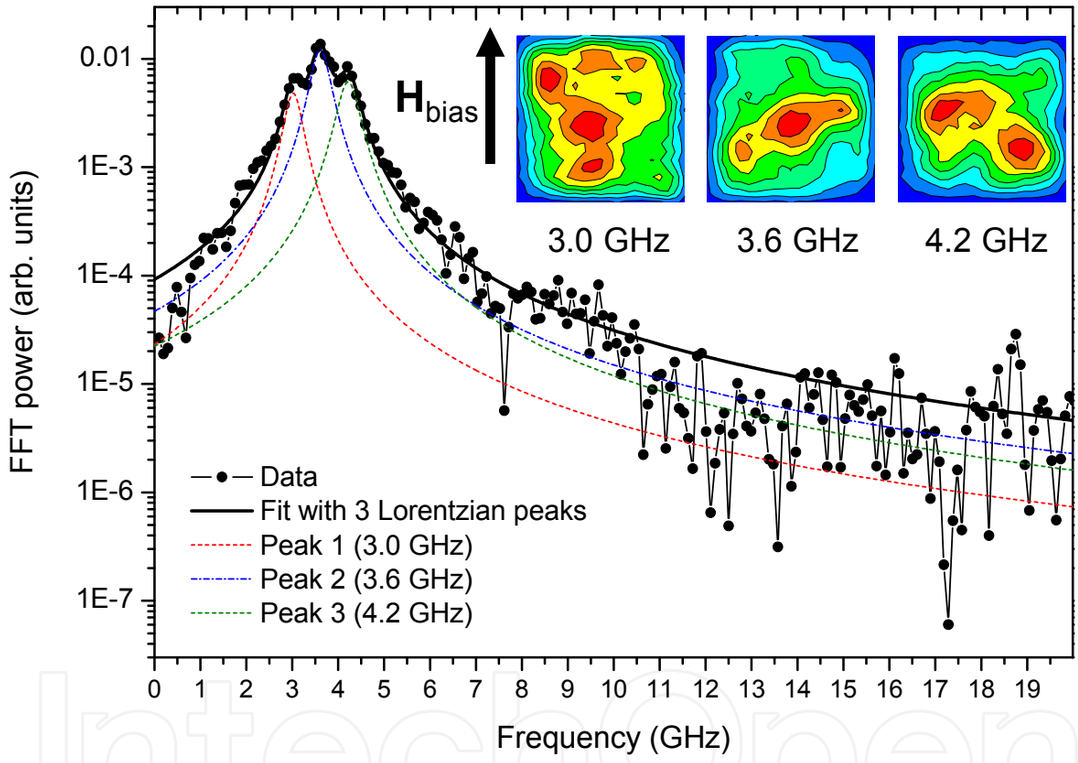

Fig. 3. The fast Fourier transform (FFT) power spectrum calculated from a time resolved Kerr signal acquired from the center of a 4 x 4 μm² array of 40 x 80 nm² stadium shaped ferromagnetic elements at a bias magnetic field of 197 Oe is shown on a logarithmic scale together with the fit to a Lorentzian 3-peak function. The inset shows images of the modes confined within the entire array and corresponding to the peak frequencies identified from the fit. The darker shades of gray correspond to greater mode amplitude. With respect to the long wavelength spin wave modes, the array acts as a continuous element made of a magnonic metamaterial. Such arrays will also act as metamaterials with respect to microwaves. After Ref. 61.

4. Band gap magnonic metamaterials

Periodically modulated magnetic materials have been shown to form magnonic crystals, i.e., a magnetic analogue of photonic crystals. Indeed, the spin wave spectrum is modified by patterning[73] and shows a tailored band structure in periodic magnetic materials[74]. The band spectrum consists of bands of allowed magnonic states and forbidden-frequency gaps ("band gaps"), in which there are no allowed magnonic states. One of the first attempts to study the propagation of spin waves in periodic magnetic structures was made by Elachi[75]. Nowadays, the number of studies on this topic has surged and continues to grow at a fast pace.

The recent advances in the studies of the band gap magnonic metamaterials are associated with advances in the Brillouin light scattering (BLS) technique, which has proved to be a very powerful tool for the investigation of magnetization dynamics in magnonic structures[76]. Thanks to the wave vector conservation in the magnon–photon interaction, one has the possibility to measure the dispersion relation (frequency versus wave vector) of spin waves. In particular, the BLS technique is suitable for measuring the magnonic band gap dispersion, provided that the periodicity of the magnonic crystal is such that the Brillouin zone (BZ) boundary lies in the accessible wave vector range (up to 2.2×10^5 rad/cm). The magnonic dispersion can be measured in different scattering geometries that differ by the relative orientation of the exchanged wave vector and direction of the applied magnetic field. So planar 1D magnonic crystals formed by arrays of closely spaced Permalloy stripes of identical[77] or alternating width[78] were studied, showing the existence of tuneable band gaps. Furthermore, alternating stripes of two different magnetic materials were studied in Ref. 79. In addition, it has recently been shown that, using a large aperture microscope objective, BLS can be used as a scanning probe technique, therefore permitting the map-out of the spatial distribution of magnonic normal modes with a lateral resolution of down to a few hundred nanometres[80,81].

The studied sample consist of long chains of Permalloy rectangular dots with rounded corners and lateral dimensions of 715 x 450 nm^2, thickness of 40 nm, edge-to-edge separation Δ = 55 nm. The magnetic material was deposited on Silicon substrate at room temperature. In our calculations, each dot was divided into cells with size $\Delta_x \times \Delta_y \times \Delta_z$ = 5 nm × 5 nm × 40 nm. The ground state was obtained using a micromagnetic code. The magnetization was assumed to be uniform in each cell and to precess around its equilibrium direction along effective field $\mathbf{H}_{\text{eff}}$. Contributions arising from the external (Zeeman), demagnetising and exchange fields were included in $\mathbf{H}_{\text{eff}}$. The following magnetic parameters obtained from the fit to the BLS frequencies of the Damon-Eshbach mode in the reference 40 nm thick continuous Permalloy film were used: saturation magnetization $4\pi M_s$ = 9 kG, $\gamma/2\pi$ = 2.94 GHz/kOe, and $A = 1.1\ 10^{-6}$ erg/cm with A being the exchange stiffness constant.

First, the collective dynamics was studied in the Voigt geometry, namely with the wave vector $\boldsymbol{q}$ perpendicular to the applied magnetic field $\mathbf{H}$ and with $\boldsymbol{q} = \boldsymbol{K}$, where $\boldsymbol{K}$ is the Bloch wave vector.

The collective modes of the array of dots were studied by using the Dynamical Matrix Method (DMM) extended to periodic magnetic systems[82]. On the basis of the number and the direction of nodal planes n = 0,1,2,.. of the dynamic magnetization inside each dot, we have classified collective modes into: the F mode with no nodal planes, Damon-Eshbach-like

(*n*DE) modes characterized by nodal planes parallel to the applied magnetic field **H**, Backward-like (*n*BA) modes with nodal planes perpendicular to **H** and *n*End-Modes (*n*EM) localized at the edges of each dot with nodal planes of the DE type.

Figure 4 (a) shows a scanning electron microscopy (SEM) image of the studied sample together with a reference frame and the directions of $\boldsymbol{q}$ and **H**. In Figure 4 (b) black lines denote frequencies of magnonic modes for $q = 0$, while the frequency curves corresponding to the edge of the first Brillouin zone (1BZ) at $q_{BZ} = \pi / a$ with a the periodicity are indicated by dashed red lines[83].

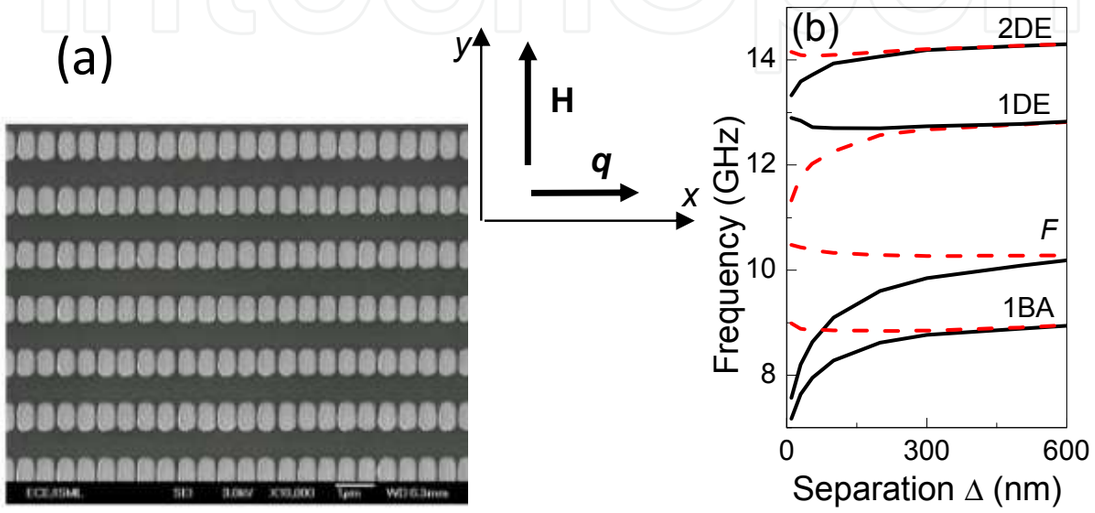

Fig. 4. (a) SEM image of the sample: Permalloy rectangular dots have lateral dimensions 715 × 450 nm² and interdot separation Δ = 55 nm. A reference frame with the direction of **H** along the *y*-axis (easy axis) and of the wave vector $\boldsymbol{q}$ is also shown. (b) Calculated frequency behaviour vs. interdot separation for the sample of dots 715 x 450 nm² in the Voigt geometry for an applied magnetic field of magnitude $H = 1$ kOe. Full black lines: frequencies at $q = 0$. Dashed red lines: frequencies at $q = \pi / a$.

As expected, for large interdot separations, each mode is characterised by a single frequency value and frequency is independent of $\boldsymbol{q}$. On decreasing the separation, interdot coupling gives rise to the appearance of bands. Due to the effect of stray magnetic field within each band the frequency of the collective modes depends on $\boldsymbol{q}$. The largest band width is that of the *F* mode that has the largest stray field at any separation. Another significant feature is the narrowing of the band gaps, as $\Delta \rightarrow 0$, either at $q = 0$ or at $q_{BZ} = \pi / a$. In particular, the band gap between the *F* and the 1DE mode is smaller for $q_{BZ} = \pi / a$, while that between the 1DE and the 2DE mode is smaller for $q = 0$. As a matter of fact, for small separation the energetic cost required to excite the F mode at $q_{BZ} = \pi / a$, namely in the anti-phase configuration, is almost the same as that of the 1-DE mode. The difference is represented by the band gap between the two modes at the 1BZ boundary. As an example the band width for a small interdot separation $\Delta = 10$ nm of the most representative modes shown in panel (b) was estimated. Calculated band width of the *F* mode turned out to be about 3.8 GHz, the largest one among those of most representative modes, but note that also the other collective modes of the spectrum have an important calculated band width in this limit (larger than 0.8 GHz).

Finally, the investigation was completed by assuming the Bloch wave vector parallel to the applied magnetic field[84]. This geometry corresponds to the so called backward volume magnetostatic spin-wave (BWVMS) geometry. In Figure 5, the dependence of the spin-wave frequencies on Δ calculated at $q = 0$ is compared to the case of $q = \pi / a$, i.e. at the edge of the 1BZ. As it can be seen, for separation values of about 300 nm, the frequencies at the centre and at the edge of the 1BZ are almost degenerate and both tend to the value of the mode frequency of an isolated dot. On reducing the value of Δ, however, the dynamic dipolar magnetic coupling becomes strong enough to remove the degeneracy. This leads to the appearance of magnonics bands whose widths increase with decreasing the interdot distance. Also in this geometry there is a narrowing of band gaps, as $\Delta \to 0$, between given couples of adjacent modes, either at $q = 0$ or at $q_{BZ} = \pi / a$.

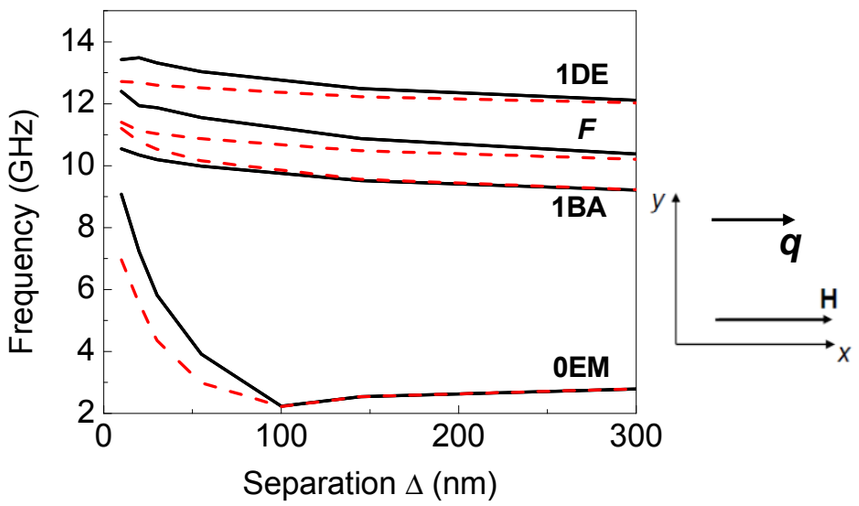

Fig. 5. Calculated mode frequencies behavior vs. interdot separation in the BWVMS geometry, i.e. for $\boldsymbol{q}$ parallel to **H**. Black lines: frequencies for $q = 0$. Dashed (red) lines: frequencies for $q_{BZ} = \pi / a$. A magnetic field of intensity $H = 1.5$ kOe was applied along the x-axis (hard axis) for the sample shown in Fig. 4 (a). The wave vector $\boldsymbol{q}$ was along the chains. The direction of $\boldsymbol{q}$ and **H** is also shown.

In particular, among the modes shown, there is a narrowing at $q_{BZ} = \pi / a$ between the 1BA and the *F* mode. Interestingly, for $\Delta < 100$ nm, the frequency increment of the 0EM is much more accentuated than that of collective modes in the higher part of the spectrum. This behaviour (which also concerns the others n-EM, not shown here) is related to the fact that the nEM are localized at some portions (typically one corner) of the adjacent edges of neighbouring dots.

2D magnonic crystals were proposed in Refs. 85,86, where the spectrum of dipole-exchange spin waves propagating in the plane of a magnonic crystal was discussed. The magnonic crystal consisted of periodically arranged infinitely long ferromagnetic cylinders embedded in a matrix of a different ferromagnetic material. The position and width of band gaps in the magnonic spectrum were investigated as a function of the period of the structure and the depth of modulation depth ("contrast") of the magnetic parameters. It was found that the

depth of modulation of the exchange parameter has a drastic effect upon the position and width of the band gaps. Collective dynamics of lattices of magnetic vortices was studied in Refs. 87,88. FMR and time resolved scanning Kerr microscopy (TRSKM) were used to study localisation of spin waves in an array of antidots formed in a metallic ferromagnetic film in Ref. 89. VNA-FMR measurements and micromagnetic simulations were used to demonstrate a control of spin wave transmission through a similar array of antidots by an external magnetic field in Refs. 90,91 (Figure 2).

The BLS technique has been exploited to achieve a complete mapping of the spin-wave dispersion curves, along the principal symmetry directions of the first BZ, for a 2D magnonic crystal consisting of a square array of 50 nm thick NiFe disks (Figure 6 (a)). The disks have a diameter d = 600 nm and are arranged in a square matrix with the edge-to-edge interdot separation of 55 nm (period a = 655 nm). This corresponds to a square first BZ of side $2\pi/a = 2\text{x}4.8 \cdot 10^4$ rad/cm. The spin-wave frequency dispersion was studied along the principal directions of the first BZ, i.e. ΓX, ΓY, XM and YM, as shown in Figure 6 (b), for external field H = 1.0 kOe applied along the [10] direction of the disk array.

In Figure 6 (c), the dispersion curves of the most representative modes are shown along the symmetry directions of the first BZ, showing a very good agreement between experimental points and calculated curves. Since the magnetic modes maintain a symmetry character similar to those found for the isolated dot, they can be labelled in the same way. Depending on the number m (n) of nodal lines perpendicular (parallel) to the direction of the magnetization (x direction), the modes are named as backward-volume-like modes m-BA (Damon-Eshbach-like n-DE), while modes with mixed character are denoted as m-BA×n-DE. The mode without nodal lines is classified as the fundamental mode (F), while modes with dynamic magnetization localized at the ends of the particle[92] are labelled as n-EM, depending on the number of nodes n. The mode type, i.e. the two indices m and n, together with the Bloch wave vector $\boldsymbol{K}$, uniquely identifies the excitation.

Figure 6 (c) shows that several modes exhibit an appreciable dispersion and are therefore propagating modes, while other modes show a frequency that remains almost constant with the wave vector, at least within the frequency resolution of the experiment. The width of each magnonic band (allowed miniband) is proportional to the mean square dynamic magnetization inside a single dot as found by DMM approach. Hence, the dispersion is largest for the F mode, while it decreases rapidly for the higher order modes, which are characterised by an increasing number of oscillations within the single dot. Starting from the Γ point, the measured frequency of the F mode increases (decreases) along the ΓY (ΓX) direction, reaching its maximum (minimum) at the Y (X) point. This behaviour reflects the properties of the dipole-exchange spin waves in the reference continuous film (open squares in Figure 6 (c)). However, the F mode is significantly downshifted with respect to the spin waves in the continuous film, which is due to the static demagnetizing field in the array along the applied field direction (x-direction). As a consequence of this in-plane anisotropy induced by the applied field, one can see that the frequency of the DE mode in the continuous film coincides near the Y-point with that of the 1-DE mode of the array. At the same time, the backward volume spin wave in the continuous film has a frequency that is in the middle of the band gap of the array, i.e. quite far from that of the corresponding 1-BA mode at X-point. In the latter point, an overlap between the F and 1-BA bands is observed.

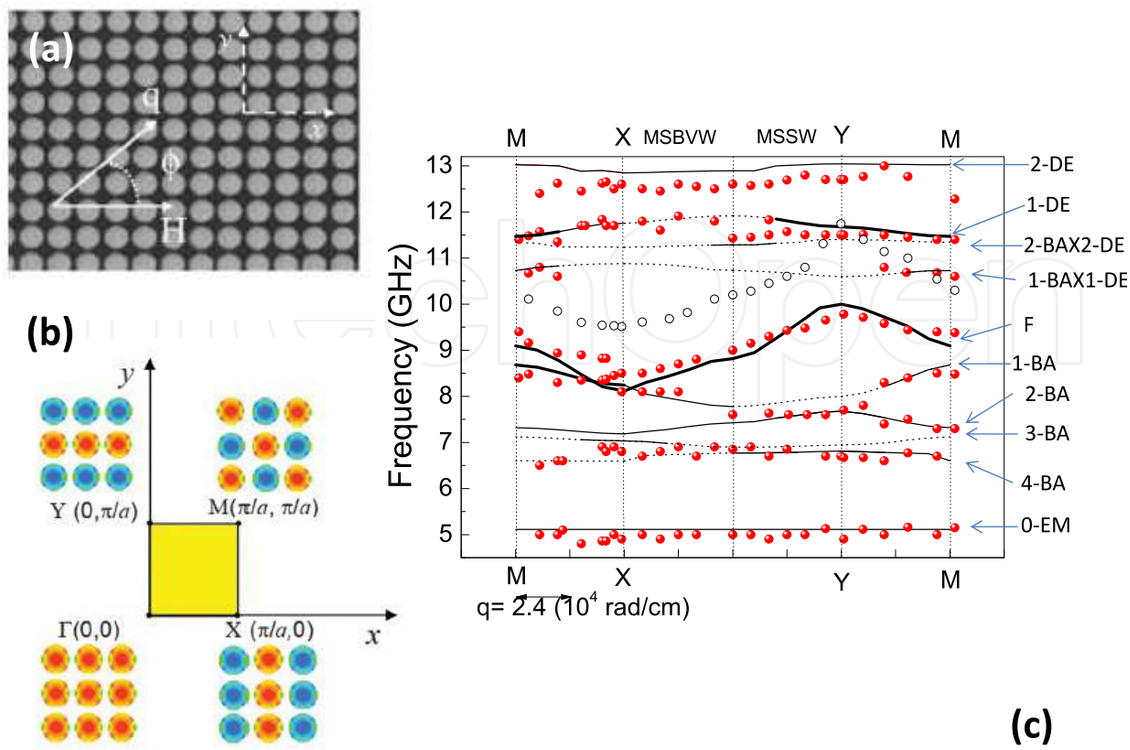

Fig. 6. (a) SEM image of the array of Permalloy disks is shown. BLS spectra were measured applying the external field H along the [10] array direction (x-axis) and changing the q_x and q_y components of the in-plane transferred wave-vector **q**. (b) Surface BZ of the 2D periodic array is shown. The behaviour of the dynamic magnetization of the fundamental mode is schematically shown in four point of the BZ for a 3x3 sub-matrix of dots. The two different colours represent out-of-plane dynamic magnetization of opposite sign. (c) Measured frequencies (dots) are shown as a function of the spin-wave wave vector along the principal direction of the first BZ, for an external magnetic field H = 1.0 kOe. The calculated dispersion curves of the most significant modes are also reported. Bold, solid or dotted lines refer to modes whose calculated cross section is comparable, smaller than 1/10 or smaller than 1/100 with respect to that of the F mode, respectively. For the sake of comparison, the experimental dispersion of the DE mode of the unpatterned film is also reported as open squares.

In Ref. [93] the dispersion of different modes was interpreted in terms of effective wave vector $\boldsymbol{k}^{\text{eff}}$ introduced as an auxiliary variable that includes and replaces the band index, i.e. the mode type, and the Bloch wave vector. It can be defined in the extended zone scheme as:

$$\boldsymbol{k}^{\text{eff}} = \boldsymbol{K} + P(m)\left[m + \frac{1-P(m)}{2}\right]\frac{\pi}{a}\hat{\mathbf{x}} + P(n)\left[n + \frac{1-P(n)}{2}\right]\frac{\pi}{a}\hat{\mathbf{y}} \qquad (1)$$

where P(*i*) is the parity function (=+1,-1 for *i* even or odd, respectively), *m*-BA×*n*-DE is the mode type, and $\boldsymbol{K}$ is assumed to vary in the reduced BZ. The effective wave vector represents the overall oscillation of the magnetization in the array, taking into account the oscillation within the dot due to the mode character (second and third terms in Eq. (1)) and the change between adjacent dots due to the Bloch wave vector (first term). The introduction

of $\boldsymbol{k}^{\text{eff}}$ helps to understand the frequency dispersion of the magnonic crystal, because, in the limit of a continuous medium, $\boldsymbol{k}^{\text{eff}}$ becomes the real wave vector of the spin excitation of the continuous film, whose dispersion curves have the following properties. The mode frequency increases (decreases) when the modulus of the wave vector increases in a direction perpendicular (parallel) to the applied field, corresponding to the MSSW (MSBVW) geometry.

To realize band gap magnonic metamaterials with a band structure of higher in-plane symmetry arrays of circular nanomagnets have been considered where an out-of-plane magnetic field stabilizes the so-called vortex state in each of the unit cells of the periodic nanodisk lattice. The dipolar interaction via nanoscale air gaps leads to allowed minibands and forbidden frequency gaps which exhibit a four-fold symmetry in in-plane directions if nanodisks are arranged in a square lattice [94]. This higher symmetry goes beyond the magnonic crystals where an in-plane field governs the symmetry of the band structure.

5. Theory of band gap magnonic metamaterials

The knowledge of the physical mechanisms which govern the dynamical behaviour of nanoscale magnetic elements is of fundamental importance for understanding the general properties of metamaterials. Because of that, the theoretical derivations of the frequency and the spatial profile of magnonic modes become necessary to gain a physical understanding of the processes observed at a macroscopic level[95-97]. Several analytical and numerical methods are used to derive the profile of normal modes. Analytical models require some preliminary assumptions (approximations) regarding the mode profiles[98,99]. Numerical tools based on micromagnetic simulations has been developed for solving the equation of motion in the time domain and to successively perform a Fourier analysis of that output signal[100,101]. The same equation can also be solved in the frequency domain. The Dynamical Matrix Method (DMM)[102] belongs to the latter approach, in which the sample is subdivided into cells and the linearized Landau–Lifshitz equation of motion is recast as a generalized eigenvalue problem, which is numerically solved by means of a finite-element method. Band structures of periodic composites can then be calculated with the help of the Bloch theorem, which reduces the number of independent variables of a periodic system to that of the corresponding unit cell[82].

The band structures of spin-waves in materials with discrete translational symmetry can be calculated also by the plane wave method (PWM). The PWM is a popular tool commonly used for studying electronic, photonic and phononic crystals because of its conceptual simplicity and applicability to any type of lattice and shape of scattering centers. The method was also adapted to the calculations of the magnonic band structures and is constantly improved, with its field of application extending to new problems[85,103]. Recently, the PWM has also been used for the calculation of spin-wave spectra of 1D magnonic crystals of finite thickness[104] and 2D thin-film magnonic crystals[105]. Only very recently, the PWM has been employed for the first time for calculating spin-wave spectra of 2D antidot arrays based on a square lattice with a good agreement with experimental results obtained[106].

The 2D magnonic crystals composed of two ferromagnetic materials in thin film geometry were studied theoretically in Refs.105,107. The plane wave method with supercell formulation was used to study the edge effect in magnonic crystals in Ref. 105. It was shown that localisation at the edges of corners of the 2D magnonic crystals with finite lateral

extension is possible. The PWM was powerful to remodel the magnonic miniband formation in short-period antidot arrays as well as the tunable metamaterial properties of large-period antidot arrays prepared in $Ni_{80}Fe_{20}$ [106,108].

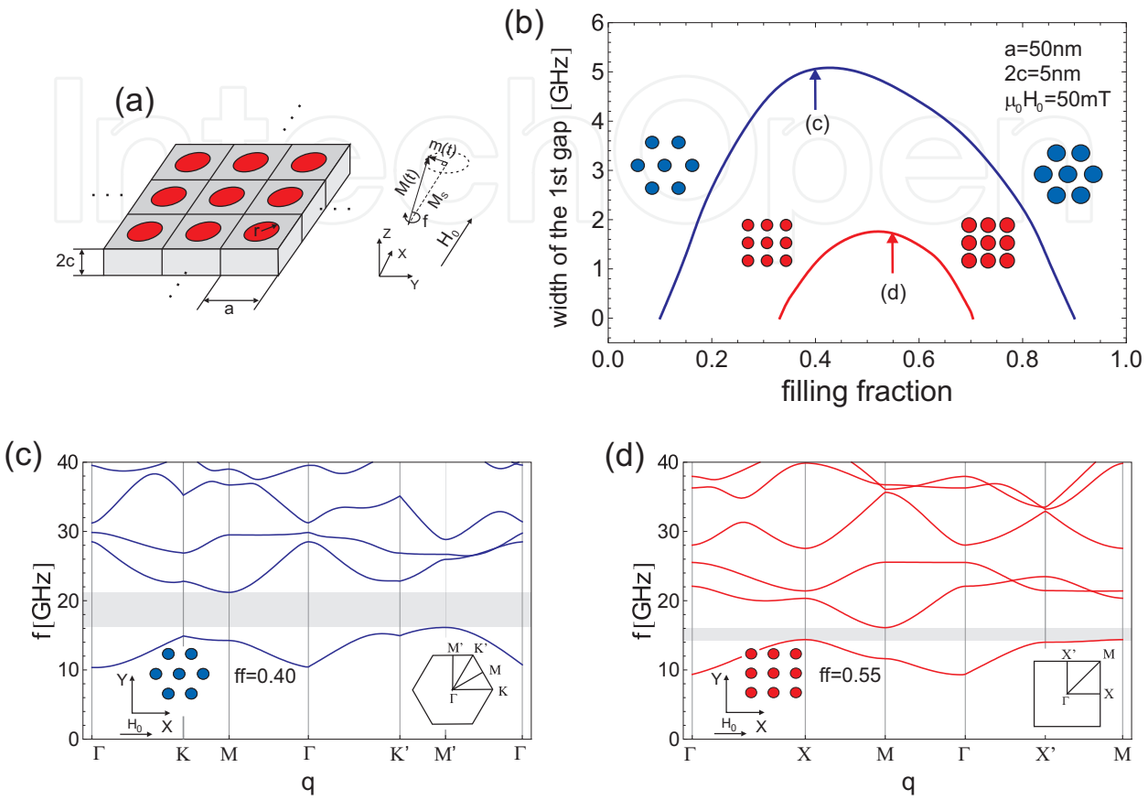

Fig. 7. The magnonic spectrum of periodic slab of finite thickness composed of the Ni inclusions embedded in Fe matrix (a) is strongly dependent on the filling fraction: the ratio of inclusion volume to the volume of unit cell, and depend on the lattice type. The maximum of the width of the first magnonic gap is reached for the intermediate values of the filling fraction (b). Note that the first absolute magnonic gap is wider for the triangular lattice (c) than for the square lattice (d).

The results of a comparative study of 2D magnonic crystals with square and triangular lattice of the Ni inclusions in Fe matrix are shown in Figure 7. The magnonic band structures for triangular and square lattices are shown in Figure 7 (c) and (d), respectively. We find that in the range of small lattice constants the triangular arrangement of cylindrical dots support opening of a magnonic gap. This gap exists for a greater range of filling fraction values and is much wider for a triangular lattice (see Figure 7 (b)). This is similar to the results of similar studies of photonic and phononic crystals. An increase of the lattice constant results in changes in mutual relation between the exchange and magnetostatic interactions. This leads to lowering frequencies of spin waves and decreasing the gap width up to closing it. In the magnetostatic regime, i.e. when the magnetostatic interactions dominate, the nonuniformity of the demagnetizing field is crucial for low frequency spin waves, especially for edge modes.

The elliptical deformation of cylindrical dots in 2D magnonic crystals was investigated in Ref. 107 by means of the plane wave method. The use of rods in the shape of elliptic cylinders as scattering centres in 2D magnonic crystals implies the introduction of two additional structural parameters: the cross-sectional ellipticity of the rods and the angle of their rotation in the plane perpendicular to the rod axis (the plane of spin-wave propagation). In contrast to the lattice constant, a change of which will strongly modify the magnonic spectrum, these new parameters allow fine tuning of the width and position of the bands and band gaps. For specific in-plane rotation angles, changing the rod ellipticity will modify the position, width, and number of bands (Figure 8). Thus, an appropriate use of rods of elliptical cross section offers additional possibilities in the design of magnonic filters with precisely adjusted passbands and stopbands.

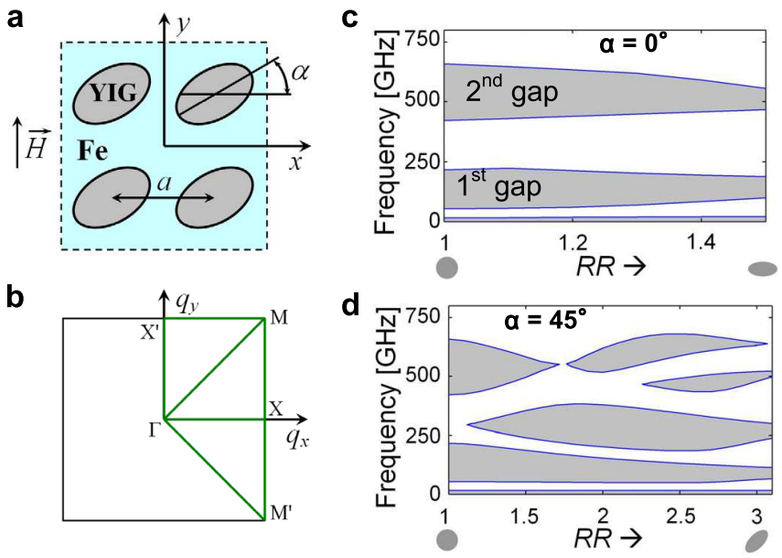

Fig. 8. Fine tuning of the magnonic band structure in the thin film 2D magnonic crystal. (a) Schematic view of the 2D magnonic crystal under study, section in the plane of periodicity. (b) High-symmetry path over the 2D Brillouin zone for ellipses arranged in a square lattice. (c)-(d) The lowest magnonic gaps (shaded) vs. rod ellipticity for 2D YIG/Fe magnonic crystals with two angles of the in-plane rotation of the rods: (c) α = 0° and (d) α = 45°. The other parameters are: lattice constant 10 nm, filling fraction 0.5, film thickness 50 nm, and external magnetic field 0.1 T.

3D band gap and effectively continuous metamaterials are the least studied objects in magnonics, due to both increased difficulty of their theoretical treatment and currently limited outlook for their fabrication and experimental investigation. Collective spin wave modes in 3D arrays of ferromagnetic particles in non-magnetic matrices were studied in Refs. 109,110. Magnonic band structure of 3D all-ferromagnetic magnonic crystals was calculated by Krawczyk and Puszkarski[111,112]. Here, again the depth of modulation of magnetic parameters is essential to generate magnonic bands and forbidden-frequency gaps of significant width.

An example of magnonic band structure for a 3D magnonic crystal resulting from the numerical solution of Landau-Lifshitz equations with the plane-wave method is shown in

Figure 9. The assumed value of the simple cubic (sc) lattice constant was 10 nm; the magnetic parameters of the matrix material were close to those of YIG, and the magnetic parameters of the ferromagnetic material of the spheres corresponded to iron. Two magnonic gaps in the resulting spectrum were observed. The first magnonic gap is delimited by the two lowest spin-wave excitations, one localized in the Fe spheres and the other in the matrix branches I and II, respectively (Figure 9 (b) and (c)). Among three cubic structures studied in Ref. 112 the magnonic crystal with face centred cubic (fcc) lattice is most suitable for gap opening.

In Ref. 113, a detailed study of all the possible combinations of 3D magnonic crystal component materials from: Co, Ni, Fe, and Py for spheres and matrix was performed to find optimal material configurations for which either absolute or partial magnonic gaps occur in the magnonic spectrum of the 3D magnonic crystal with hexagonal structure. Among the MCs considered in this study, an absolute magnonic gap is obtained in a crystal with Ni spheres embedded in Fe.

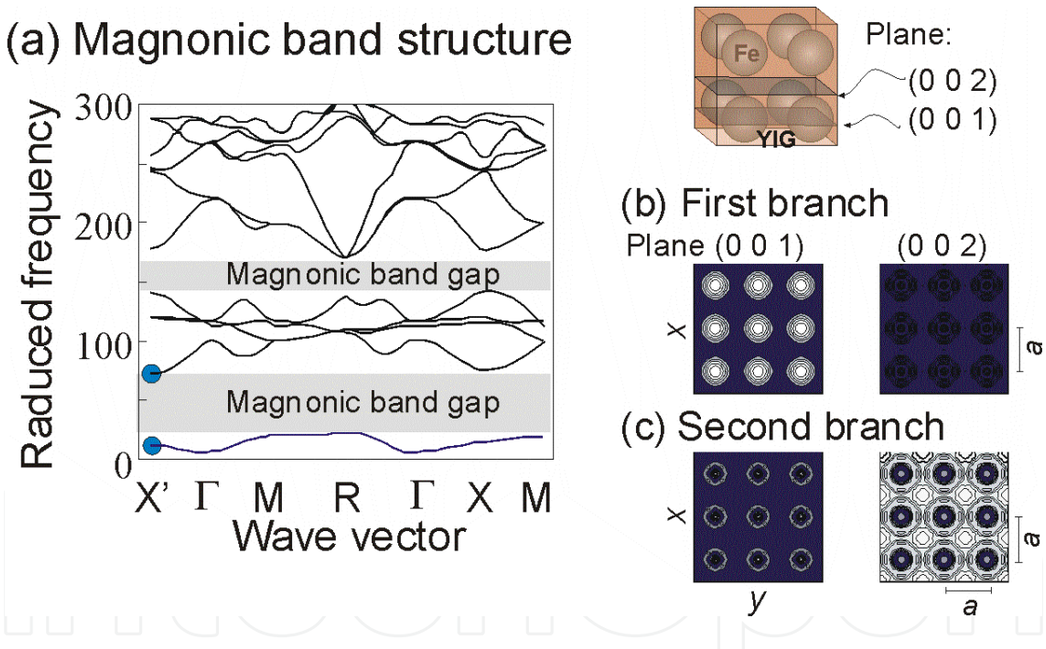

Fig. 9. (a) The magnonic band structure of a simple cubic (sc) magnonic crystal with a lattice constant of 10 nm. The magnonic crystal is composed of Fe spheres of radius 26.28 Å disposed in sites of the sc lattice and embedded in YIG. Blue circles indicate the beginnings of the first two branches at point at which profiles of spin-waves are shown in (b) and (c). (b) and (c) Profiles of squared dynamic magnetization component in two adjacent planes, (002) and (001) right and left column, respectively. The planes are shown in the inset on the top-right. White colour corresponds to maximum values of amplitudes dynamic magnetization. Reproduced from Ref. 112. Copyright 2008, American Physical Society.

Using the method from Refs. 112 and 113, we performed calculations for 3D magnonic crystals based on magnetoferritin crystals (mFT) described in the next section. In the calculations, we assumed mFT spheres (diameter 8 nm) in fcc lattice (with lattice constant 14 nm) immersed in Co. Assuming magnetic and structural parameters taken from literature for dehydrated mFT crystals and cobalt, we showed in Figure 10 (a) that a wide absolute magnonic band gap should exist in the magnonic spectrum of the structure, well above 100 GHz. It means that replacing the protein shell in magnetoferritin crystals with ferromagnetic metals should allow for opening the magnonic band gap. The gap is absolute and wide, and so, it is very promising for application of 3D magnonic crystals.

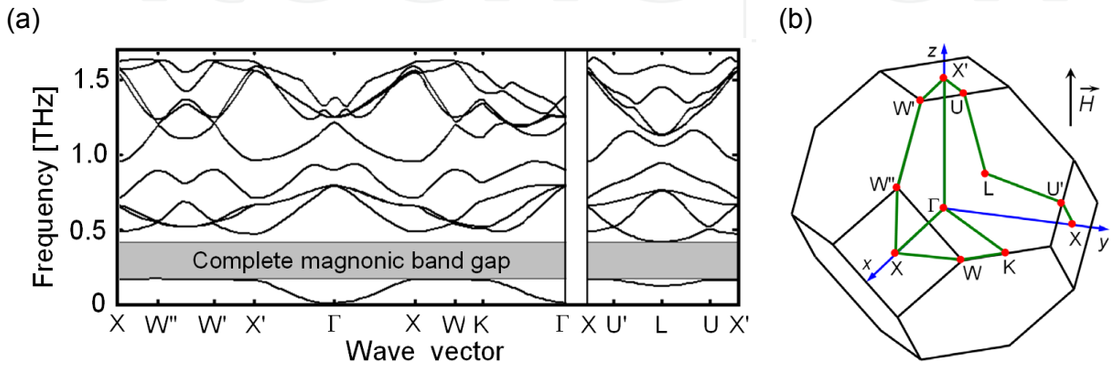

Fig. 10. (a) The magnonic band structure of fcc magnonic crystal with lattice constant of 14 nm is shown. The magnonic crystal is composed of magnetoferritin spheres of diameter 8 nm embedded in Co. The external bias magnetic field 0.1 T is applied along z-axis. (b) First Brillouin zone of the fcc lattice, with the path along which we calculate the magnonic band structure in (a).

The magnonic dispersion can also be calculated from the results of micromagnetic simulations by Fourier transforming them in both temporal and spatial dimensions into the reciprocal space. For 1D samples, the method was realised in Ref. 16, and then used in a number of further studies[114,115]. So, Figure 11 shows the magnonic dispersion of a stack of dipolarly coupled magnetic nanoelements, studied in Ref. 115. The sign of the magnonic dispersion along the stacking direction is determined by the spatial character and ellipticity of the corresponding modes of an isolated nanoelement. Moreover, there exists a critical value of the ellipticity at which the sign of the magnonic dispersion changes from negative to positive in a discontinuous way. The discovered effect suggests a novel way of tailoring the dispersion of collective spin waves in magnonic bandgap metamaterials, unique to magnonics.

Reprogrammable dynamic response has been demonstrated through different remanent states of planar arrays of nanomagnets[116]. The reconfiguration of a 1D magnonic crystal has recently been demonstrated via variation of the orientation of neighbouring ferromagnetic nanowires from a parallel to anti-parallel magnetic states (Figure 12)[117,118]. Experiments and simulations have shown that spin waves propagating perpendicular to the long axis of such coupled nanowires experience different artificial magnonic band structures in configurations (a) and (b). Magnonic dispersions have thus become reprogrammable.

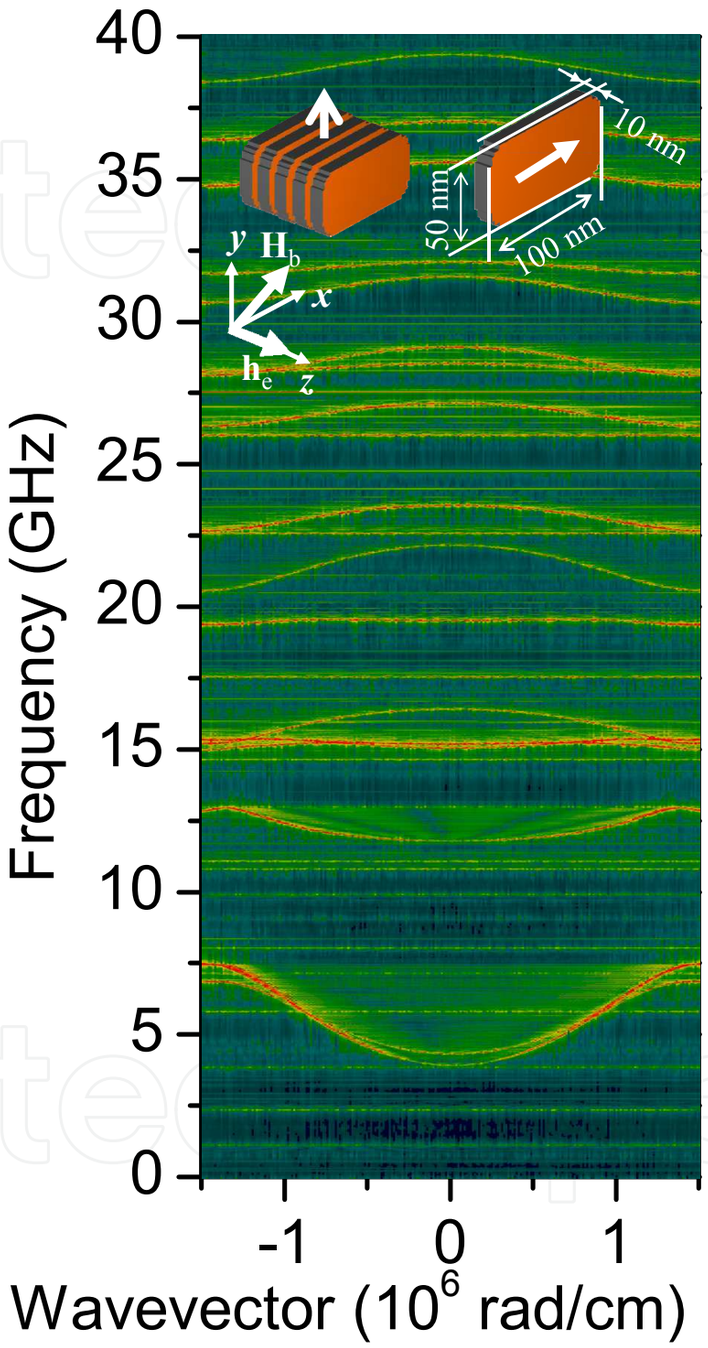

Fig. 11. The magnonic dispersion is shown for a stack of 240 stadium shaped magnetic elements with dimensions of 100x50x10 nm^3. The inset schematically shows the studied sample and geometry of the problem. After Ref. 115.

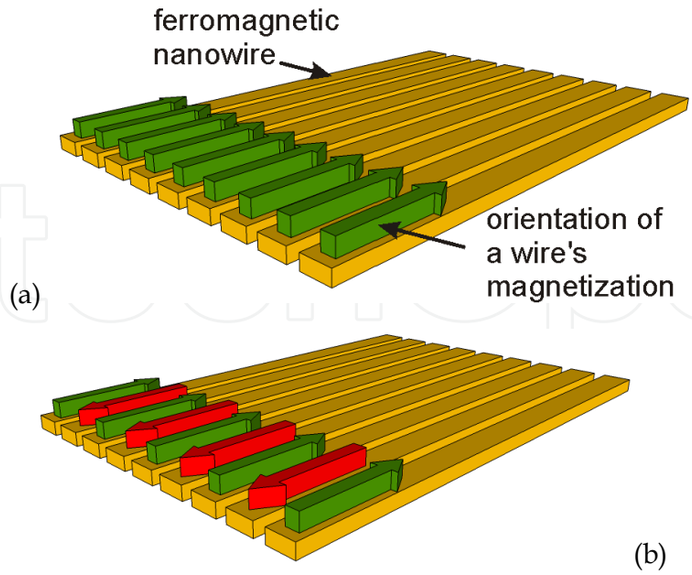

Fig. 12. Two different remanent magnetic configurations of a 1D magnonic crystal formed by interacting ferromagnetic nanowires are shown for (a) parallel and (b) anti-parallel alignment of neighbouring nanowires. In (b), the magnetic unit cell of the magnonic crystal is twice as large as the geometrical one, leading to zone folding effects of magnon dispersions in the reciprocal space [117].

6. Theory of effectively continuous magnonic metamaterias

The theory of the effective properties of magnonic metamaterials in situations when they behave as "effectively continuous" can often be derived as the long wavelength limit of the corresponding band gap theory. The latter can however be quite complex, so that it becomes more practical and useful to develop the effectively continuous theory without a reference to the band gap one. In the case of the effective permeability of magnetic composites and metamaterials, the majority of analytical models employ the so-called macrospin approximation, in which each magnetic inclusion within a non-magnetic matrix is considered as a single giant spin and is therefore characterized by a single magnetic resonance. However, it is well known that the spin wave spectrum of magnetic nano-structures and nano-elements has a complex structure, featuring series of resonances due to spatially non-uniform spin wave modes[54-56,61,64,67-69,71,92-99,115,119]. Each of the resonances is expected to contribute to the susceptibility tensor of the magnetic constituents and correspondingly to the permeability tensor of the whole metamaterial. The resonance frequencies can be controlled and reconfigured by the external magnetic[119-121] and electric[122,123] fields, and the same functionalities should therefore be inherited by the magnonic metamaterials.

A method of calculation of the effective permeability that takes full account of the complex spectrum of the metamaterial's individual magnetic constituents has been demonstrated in

Ref. 59. In this method, the susceptibility tensor of an isolated inclusion is calculated numerically and then used as an input to an analytical expression (a so-called "mixing rule") for the permeability of the whole metamaterial. Finding the susceptibility tensor of the isolated inclusion is a standard problem for micromagnetics, and can be addressed using a number of different approaches. For example, full-scale numerical micromagnetic simulations could be performed using one of the available micromagnetic packages (e.g. Nmag[124], OOMMF[125], or MicroMagus[126]). Alternatively, the dynamical matrix method, which has already been introduced above, can be used a form modified to facilitate the susceptibility calculations. The results of the application of the method to a model metamaterial representing an array of magnetic nanodisks embedded into a non-magnetic matrix (inset in Figure 13) is shown in Figure 14. Figure 13 shows the region of geometrical parameters of such a metamaterial, in which one of the components of the permeability tensor becomes negative within a certain frequency range. The method also presents a useful way by which to compare the different micromagnetic methods in order to evaluate the accuracy to be expected from micromagnetic simulations. In particular, we find that the results produced by the state-of-art micromagnetic simulations agree with each other within an error bar of about 5%, which has to be taken into account when micromagnetic calculations are used to model experimental data.

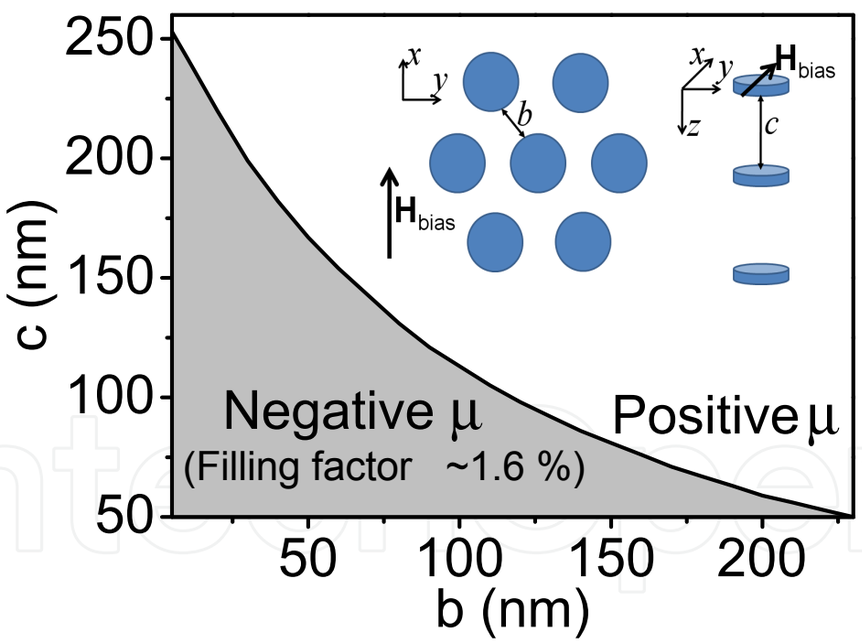

Fig. 13. The range of values of the in-plane edge-to-edge separation (b) and the distance between layers (c) in which μ_{yy} component of the permeability becomes negative near the frequencies of the dominant magnonic resonances. The inset shows the geometry of the metamaterial consisting of magnetic discs in a non-magnetic matrix. The discs are located in nodes of a hexagonal lattice. The disk diameter is d = 195 nm, the in-plane edge-to-edge separation is b = 20 nm, the distance between the layers is c = 140 nm and is much greater than disk thickness l = 5 nm.

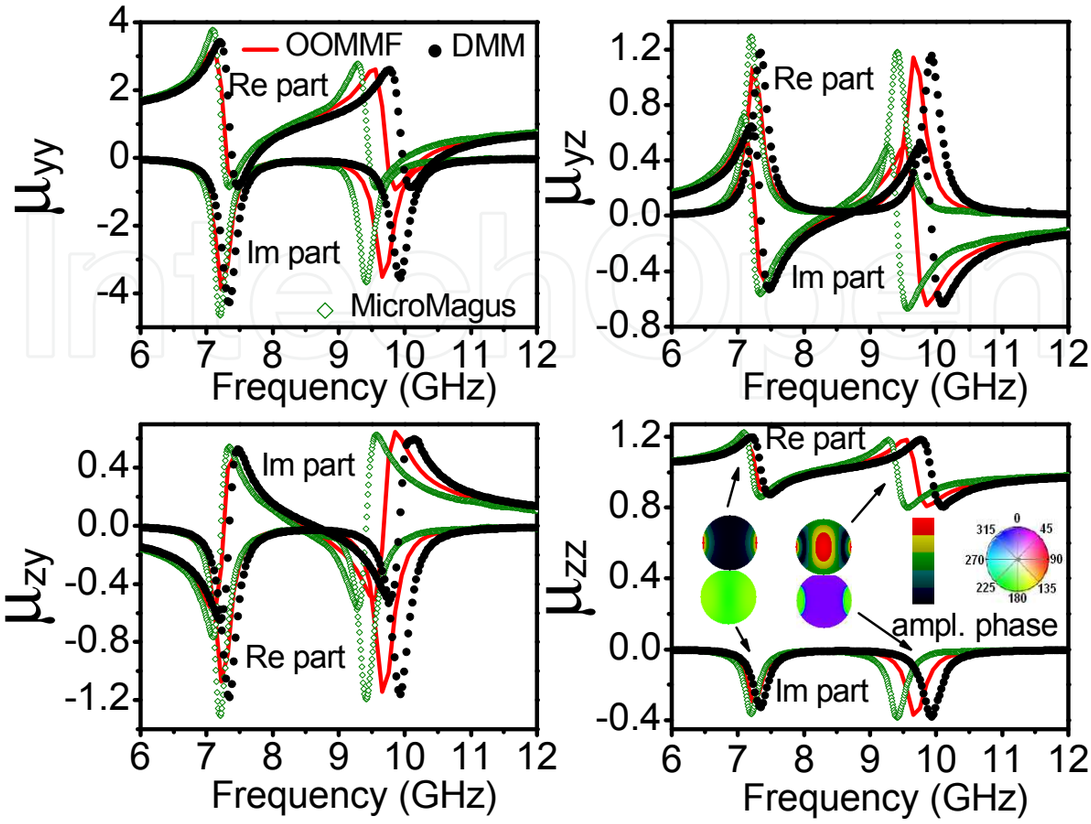

Fig. 14. The real and imaginary parts of the four components of the effective permeability tensor are shown as functions of frequency for the metamaterial depicted in Figure 13. The filling factor is 2.48% and the constant external magnetic field is H_{bias} = 933 Oe. The field is applied in the plane of the layers along the x axis. The insets show the spatial profiles of the mode amplitude (top) and phase (bottom) for the two dominant modes.

7. Bottom-up technologies for metamaterials

In the context of nanostructured magnonic metamaterials, the main nanomanufacturing challenge is to fabricate large-scale periodic structures consisting of or containing magnetic materials precisely and controllably tailored at the nanometre scale. Being at the limit of current lithographic tools, the challenge requires bottom-up technologies be exploited instead. For example, protein based colloidal crystallisation techniques can be used to produce macroscopic 3D ordered magnetic arrays[127,128].

There are a number of possible ways to achieve a periodic 3-dimensional magnetic structure. Apart from top-down lithography, which is generally limited to structures with a height much less than their in-plane dimensions, self-assembly offers a number of promising routes. For example, a number of researchers have used colloidal crystallization to generate periodic 3-dimensional arrays of magnetic nanoparticles[129]. A variation of this approach, which has the advantage that it separates nanoparticle functionality and array formation, exploits the ability of certain proteins both to act as templates for nanoparticle formation and to crystallize. The first demonstration of this method used the ubiquitous iron

storage protein ferritin as a template for the growth of ferrimagnetic magnetite-maghemite nanoparticles[127,130]. Ferritin consists of a spherical protein shell with an outer diameter of 12 nm and an inner diameter of 8 nm, and the *in vivo* incorporation of Fe into apoferritin (ferritin without its mineral core) is achieved by the oxidation of Fe^{2+} ions transported through its ion channels.

Following magnetite nanoparticle synthesis, the magnetoferritin (this is the name given to ferritin containing a synthetic ferrimagnetic core) is purified by ion-exchange chromatography, and then passed through a stainless-steel-packed column in a uniform 0.7-0.8 T magnetic field to separate any protein including non- or poorly-magnetic nanoparticles from the magnetoferritin. In a further purification stage size-exclusion chromatography is used to separate magnetoferritin monomers from dimers and oligomers before crystallization, which used the sitting-drop vapour diffusion technique and Cd^{2+} as a crystallization agent. A schematic of this process is shown in Figure 15.

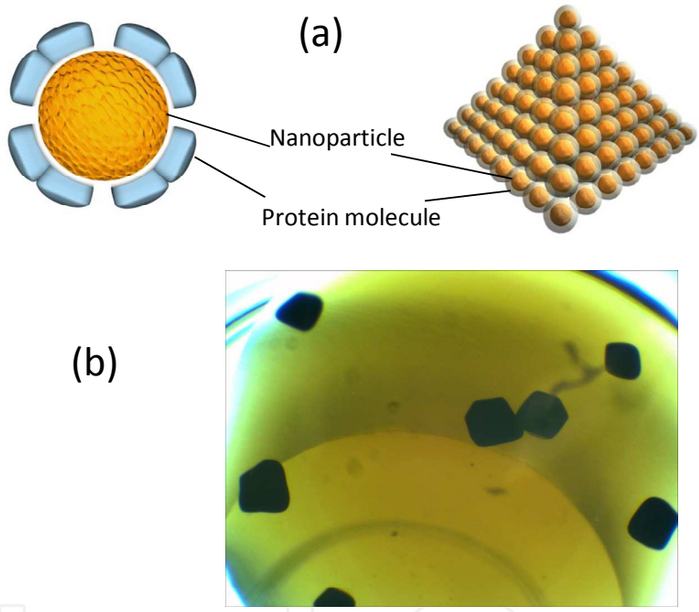

Fig. 15. (a) Schematic showing how crystallizing a protein used as a template for nanoparticle growth gives a periodic 3D array of nanoparticles. (b) Optical image showing magnetoferritin crystals. Each crystal is a periodic 3-dimensional array of magnetite nanoparticles.

To study the metamaterials properties of several magnetoferritin crystals in parallel, fifty of the as-prepared crystals were mounted on a coplanar waveguide (CPW) in order to perform all electrical spin-wave spectroscopy[131,132]. In contrast to earlier studies on nanoparticle arrays where a microwave cavity at a fixed frequency was used[133,134], the CPW-based technique allows one to measure over a broad frequency range. The CPW with the magnetoferritin crystals on top of it is shown in Figure 16. Using a VNA, which is connected to the CPW via microwave probe tips, we apply a microwave current to the CPW. This provokes a microwave magnetic field $\mathbf{h}_{rf}$ around the inner conductor of the CPW. Considering the frequencies ranging from 10 MHz up to 26.5 GHz, we address spin

excitations in the magnetoferritin crystals when exploring the metamaterials properties. Using a 20 μm wide inner conductor, we excite spin waves with a distribution of wave vectors **k** given by the current distribution through the CPW[135]. Experiments are carried out in a cryogenic setup allowing us to perform measurements over a wide temperature range with an external field of up to 2.5 T. The field is applied in a direction perpendicular to the plane of the CPW. This direction is chosen so that torque $\boldsymbol{\tau} \sim \mathbf{M} \times \mathbf{h}_{rf}$ is maximised when **M** ($\mathbf{h}_{rf}$) is out-of-plane (in-plane). Torque $\boldsymbol{\tau}$ excites the spin waves.

We start our discussion from room temperature data taken at 290 K (Figure 16). We measure the dynamic response as a function of applied external field. We observe pronounced absorption with a linear dependency indicated by the white dashed line. Interestingly, the resonance starts to appear at fields larger than 0.1 T, whereas at 0 T there is no resonance observed. We attribute the observed behaviour to the paramagnetic response of the protein crystals, in which the magnetization vectors of the nanoparticles are randomly aligned at zero field. An anisotropy term does not seem to be present to provoke a non-zero resonance frequency at small field. The individual nanoparticles show superparamagnetic behaviour, which is expected for particles of this size.

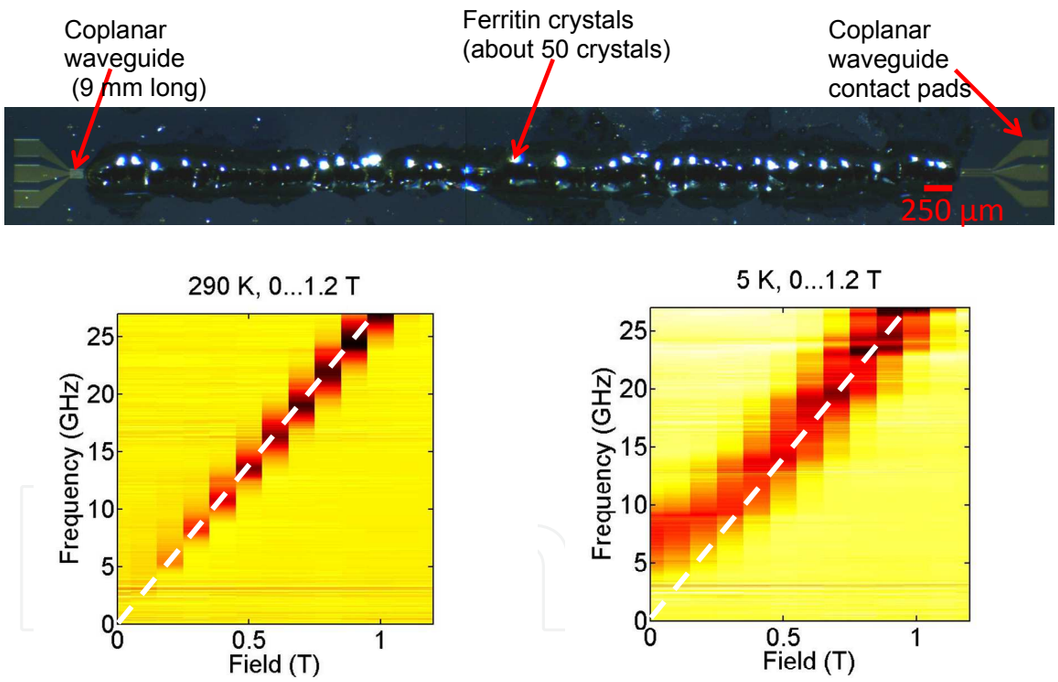

Fig. 16. (Top) Microscopy image of the 9 mm long coplanar wave guide containing 50 magnetoferritin crystals as shown in Figure 15. (Bottom) Spectroscopy data taken at 290 K (left) and 5 K (right) as a function of perpendicular magnetic field. Dark colour indicates spin-wave excitation. The broken lines are guides for the eyes reflecting both the field dependency at 290 K to facilitate comparison.

The data at 5 K show a different behaviour, as we observe a clear absorption peak even at zero field. Here, the resonance is measured to be at 6 GHz. For fields larger than about 0.5 T, we observe a linear dependence of the resonance frequency with the applied field as well,

but it is slightly shifted towards higher frequencies if compared to the room temperature measurement (white dashed line). The resonance frequency at zero field implies an anisotropy term aligning spins even without external field.

In order to use 3D nanoparticle assemblies as all-magnetic metamaterials, it would be relevant that researchers combine the protein based nano-manufacturing with advanced 3D material deposition techniques such as atomic layer deposition (ALD)[136] and electrodeposition tailored for use with multiple magnetic materials. From this all-ferromagnetic 3D magnonic metamaterials might result. ALD film growth is self-limited, thereby achieving atomic scale control of the deposition. Recently, ALD was used to deposit ferromagnetic thin-films (such as Ni, Co, Fe_3O_4) into deep-etched trenches and membranes[137,138,139]. The complementary topology is also possible by, e.g., conformal coating of templates consisting of tailored nanowires[140]. Such possibilities make ALD a promising tool by which to fabricate 3D magnonic devices. Electrodeposition is also very well suited for deposition into complex templates[141]. It is fast and thereby suitable for scaling-up to produce large numbers of devices. For example, arrays of cylindrical magnetic nanowires deposited electrochemically within porous membranes[142,143,144] have attracted much attention due to their potential for use as microwave[145] and THz[13] devices.

8. Conclusions

The modern research on fundamental properties of materials is increasingly driven by their anticipated potential for technological applications. In this Chapter, we have reviewed research that has been conducted within the MAGNONICS project funded by the European Commission to reveal the potential of magnonic metamaterials nanoscale building blocks of which are made of magnetic materials. A particular attention is devoted to the use of spin wave resonances tailored in magnonic crystals for design of novel features in the electromagnetic properties in the GHz-THz frequency range. These entirely new electromagnetic metamaterials could be designed to tune the transmission, absorption and reflection of electromagnetic radiation in the GHz-THz frequency range. Such magnonic metamaterials could also find their use within magnonic filters and logic gates.

The field of magnonics and magnonic metamaterials is very young. However, the growing community of magnonics researchers has already demonstrated that they are up to the challenges existing in the magnonics science and technology. In particular, this Chapter demonstrates important advances recently achieved in the direction of the development of effectively continuous and band gap magnonic metamaterials.

9. Acknowledgments

We thank S. Neusser for providing simulation results, P. Berberich, G. Duerr, R. Huber, J. Topp, and T. Rapp for experimental support. The authors gratefully acknowledge funding received from the European Community's Seventh Framework Programme (FP7/2007-2013) under Grant Agreements no 233552 (DYNAMAG) and 228673 (MAGNONICS), from the Engineering and Physical Sciences Research Council (EPSRC) of United Kingdom (project EP/E055087/1), from the German excellence cluster "Nanosystems Initiative Munich (NIM)".

10. References

[1] A. De Baas (Editor), "Nanostructured metmaterials" (The European Commission, Publications Office, 2010).
[2] V. G. Veselago, Sov. Phys. Uspekhi 10, 509 (1968).
[3] J. B. Pendry, D. Schurig, and D. R. Smith, Science 312, 1780 (2006).
[4] J. B. Pendry, Phys. Rev. Lett. 85, 3966 (2000).
[5] J. B. Pendry, A. J. Holden, D. J. Robbins, and W. J. Stewart, IEEE Trans. Microwave Theory Tech. 47, 2075 (1999).
[6] O. Acher, J. Magn. Magn. Mater. 321, 2093 (2009).
[7] R. V. Mikhaylovskiy, E. Hendry, and V. V. Kruglyak, Phys. Rev. B 82, 195446 (2010).
[8] A. G. Gurevich and G. A. Melkov, Magnetization oscillations and waves (CRC Press, 1996).
[9] V. V. Kruglyak, S. O. Demokritov, and D. Grundler, J. Phys. D: Appl. Phys. 43, 264001 (2010).
[10] A. Aharoni, J. Appl. Phys. 69, 7762 (1991); *ibid*. 81, 830 (1997).
[11] D. Mercier, J. - C. S. Levy, G. Viau, F. Fievet-Vincent, F. Fievet, P. Toneguzzo, and O. Acher, Phys. Rev. B 62, 532 (2000).
[12] J. Ramprecht and D. Sjöberg, J. Phys. D – Appl. Phys. 41, 135005 (2008).
[13] G. S. Makeeva, M. Pardavi-Horvath, and O. A. Golovanov, IEEE Trans. Magn. 45, 4074 (2009).
[14] V. Boucher, L. – P. Carignan, T. Kodera, C. Caloz, A. Yelon, and D. Ménard, Phys. Rev. B 80, 224402 (2009).
[15] V. V. Kruglyak and A. N. Kuchko, J. Magn. Magn. Mater. 272-276, 302 (2004).
[16] V. V. Kruglyak and R. J. Hicken, J. Magn. Magn. Mater. 306, 191 (2006).
[17] E. Yablonovitch, Phys. Rev. Lett., 58, 2059 (1987).
[18] W. L. Barnes, A. Dereux, and T. W. Ebbesen, Nature (London) 424, 824 (2003).
[19] L. M. Brekhovskikh and O. A. Godin, *Acoustics Of Layered Media I: Plane And Quasi-Plane Waves* (Springer-Verlag, Berlin, 1990).
[20] S. A. Nikitov, P. Tailhades, and C. S. Tsai, J. Magn. Magn. Mater. 236, 320 (2001).
[21] S. Tamaru, J. A. Bain, R. J. M. van de Veerdonk, T. M. Crawford, M. Covington, and M. H. Kryder, Phys. Rev. B 70, 104416 (2004).
[22] V. E. Demidov, B. Hillebrands, S. O. Demokritov, M. Laufenberg, and P. P. Freitas, J. Appl. Phys. 97, 10A717 (2005).
[23] Z. Liu, F. Giesen, X. Zhu, R. D. Sydora, and M. R. Freeman, Phys. Rev. Lett. 98, 087201 (2007).
[24] J. Gouzerh, A. A. Stashkevich, N. G. Kovshikov, V. V. Matyushev, and J. M. Desvignes, J. Magn. Magn. Mater. 101, 189 (1991).
[25] Y. I. Gorobets and S. A. Reshetnyak, Techn. Phys. 43, 188 (1998).
[26] A. M. Kuchko, Metallofiz. Noveish. Tekhn. 27, 511 (2005).
[27] A. V. Vashkovsky and E. H. Lock, Phys. Uspekhi 49, 389 (2006).
[28] S. K. Kim, S. Choi, K. S. Lee, D. S. Han, D. E. Jung, and Y. S. Choi, Appl. Phys. Lett. 92, 212501 (2008).
[29] V. E. Demidov, S. O. Demokritov, D. Birt, B. O'Gorman, M. Tsoi, and X. Li, Phys. Rev. B 80, 014429 (2009).
[30] A. V. Vashkovskii, K. V. Grechushkin, A. V. Stalmakhov, and V. A. Tyulukin, Radiotekhn. Elektronika 32, 2295 (1987).

[31] V. K. Dugaev, P. Bruno, B. Canals, and C. Lacroix, Phys. Rev. B 72, 024456 (2005).
[32] S. Yang, Z. Song, and C. P. Sun, Europ. Phys. J. B 52, 377 (2006).
[33] S. K. Choi, K. S. Lee, and S. K. Kim, Appl. Phys. Lett. 89, 062501 (2006).
[34] K. Perzlmaier, G. Woltersdorf, and C. H. Back, Phys. Rev. B 77, 054425 (2008).
[35] D. R. Birt, B. O'Gorman, M. Tsoi, X. Li, V.E. Demidov, and S.O. Demokritov, Appl. Phys. Lett. 95, 122510 (2009).
[36] F. Morgenthaler, IEEE Trans. Magn. MAG8, 550 (1972).
[37] V. S. L'vov, A. M. Rubenchik, V. V. Sobolev, and V. S. Synakh, Fiz. Tverd. Tela 15, 793 (1973).
[38] O. Büttner, M. Bauer, S. O. Demokritov, B. Hillebrands, Y. S. Kivshar, V. Grimalsky, Y. Rapoport, M. P. Kostylev, B. A. Kalinikos, and A. N. Slavin, J. Appl. Phys. 87, 5088 (2000).
[39] R. Khomeriki, Europ. Phys. J. B 41, 219 (2004).
[40] V. Verrakumar and R. E. Camley, IEEE Trans. Magn. 42, 3318 (2006).
[41] V. E. Demidov, J. Jersch, S. O. Demokritov, K. Rott, P. Krzysteczko, and G. Reiss, Phys. Rev. Lett. 102, 177207 (2009).
[42] S. O. Demokritov, A. A. Serga, A. Andre, V. E. Demidov, M. P. Kostylev, B. Hillebrands, and A. N. Slavin, Phys. Rev. Lett. 93, 047201 (2004).
[43] A. Kozhanov, D. Ouellette, M. Rodwell, S. J. Allen, A. P. Jacob, D. W. Lee, and S. X. Wang, J. Appl. Phys. 105, 07D311 (2009).
[44] E. A. Vilkov, Phys. Solid State 48, 1754 (2006).
[45] D. D. Stancil, B. E. Henty, A. G. Cepni, and J. P. Van't Hof, Phys. Rev. B 74, 060404 (2006).
[46] V. Vlaminck and M. Baileul, Science 322, 410 (2008).
[47] A. M. Kosevich, B. A. Ivanov, and A. S. Kovalev, Phys. Rep. 194, 117 (1990).
[48] A. N. Slavin, S. O. Demokritov, and B. Hillebrands, Top. Appl. Phys. 83, 35 (2002).
[49] Y. K. Fetisov, C. E. Patton, and V. T. Synogach, JETP Lett. 83, 488 (2006).
[50] M. Z. Wu, P. Krivosik, B. A. Kalinikos, and C. E. Patton, Phys. Rev. Lett. 96, 227202 (2006).
[51] M. H. Seavey and P. E. Tannenwald, Phys. Rev. Lett. 1, 168 (1958).
[52] C. Kittel, Phys. Rev. 110, 1295 (1958).
[53] C. Mathieu, J. Jorzick, A. Frank, S. O. Demokritov, A. N. Slavin, B. Hillebrands, B. Bartenlian, C. Chappert, D. Decanini, F. Rousseaux, and E. Cambril Phys. Rev. Lett. 81, 3968 (1998).
[54] A. Barman, V. V. Kruglyak, R. J. Hicken, J. M. Rowe, A. Kundrotaite, J. Scott, and M. Rahman, Phys. Rev. B 69, 174426 (2004).
[55] M. Bailleul, R. Höllinger, K. Perzlmaier, and C. Fermon, Phys. Rev. B 76, 224401 (2007).
[56] I. Neudecker, F. Hoffmann, G. Woltersdorf, and C. H. Back, J. Phys. D – Appl. Phys. 41, 164010 (2008).
[57] K.-D. Lee, J.-W. Kim, J.-W. Jeong, S.-C. Shin, J. Appl. Phys. 106, 113904 (2009).
[58] M. Krawczyk, J. Magn. Magn. Mater. 322, 562 (2010).
[59] O. Dmytriiev et al (unpublished).
[60] J. H. E. Griffiths, Nature (London) 158, 670 (1946).
[61] V. V. Kruglyak, P. S. Keatley, A. Neudert, R. J. Hicken, J. R. Childress, and J. A. Katine, Phys. Rev. Lett. 104, 027201 (2010).
[62] H. Al-Wahsh, Eur. Phys. J. B 73, 527-537 (2010).

[63] R. E. Camley, M. R. F. Jensen, S. A. Feiven, and T. J. Parker, J. Appl. Phys. 83, 6280 (1998).
[64] F. Giesen, J. Podbielski, B. Botters, and D. Grundler, Phys. Rev. B 75, 184428 (2007).
[65] S. S. Kalarickal, P. Krivosik, M. Wu, C. E. Patton, M. L. Schneider, P. Kabos, T. J. Silva, and J. P. Nibarger, J. Appl. Phys. 99, 093909 (2006).
[66] M. Belmeguenai, T. Martin, G. Woltersdorf, M. Maier, and G. Bayreuther, Phys. Rev. B 76, 104414 (2007).
[67] W. K. Hiebert, A. Stankiewicz, and M. R. Freeman, Phys. Rev. Lett. 79, 1134 (1997).
[68] R. J. Hicken, A. Barman, V. V. Kruglyak, and S. Ladak, J. Phys. D: Appl. Phys. 36, 2183 (2003).
[69] C. H. Back, D. Pescia, and M. Buess, Top. Appl. Phys. 101, 137 (2006), and references therein.
[70] J. Li, M.-S. Lee, W. He, B. Redeker, A. Remhof, E. Amaladass, C. Hassel, and T. Eimueller, Rev. Sci. Instr. 80, 073703 (2009).
[71] P. S. Keatley, V. V. Kruglyak, A. Neudert, M. Delchini, R. J. Hicken, J. R. Childress, and J. A. Katine, J. Appl. Phys. 105, 07D308 (2009).
[72] M. L. Schneider, J. M. Shaw, A. B. Kos, T. Gerrits, T. J. Silva, and R. D. McMichael, J. Appl. Phys. 102, 103909 (2007).
[73] B. Hillebrands and A. Thiaville (Eds.), *Spin dynamics in Confined Structures I-III* (Springer, 2001-2006).
[74] G. Gubbiotti, S. Tacchi, G. Carlotti, N. Singh, S. Goolaup, A. O. Adeyeye, and M. Kostylev, Appl. Phys. Lett. 90, 092503 (2007).
[75] C. Elachi, IEEE MAG-11, 36 (1975).
[76] G. Gubbiotti, S. Tacchi, M. Madami, G. Carlotti, A. O. Adeyeye, and M. Kostylev, J. Phys. D: Appl. Phys. 43, 264003 (2010).
[77] G. Gubbiotti, S. Tacchi, G. Carlotti, N. Singh , S. Goolaup , A. O. Adeyeye, and M. Kostylev, Appl. Phys. Lett. 90, 092503 (2007).
[78] S. Tacchi, M. Madami, G. Gubbiotti, G. Carlotti, S. Goolaup, A. O. Adeyeye, N. Singh and M. P. Kostylev, Phys. Rev. B 82, 184408 (2010).
[79] Z. K. Wang, V. L. Zhang, H. S. Lim, S. C. Ng, M. H. Kuok, S. Jain, and A. O. Adeyeye, Appl. Phys. Lett. 94, 083112 (2009).
[80] G. Gubbiotti, G. Carlotti, M. Madami, S. Tacchi, P. Vavassori, and G. Socino, J. Appl. Phys. 105, 07D521 (2009).
[81] M. Madami, S. Bonetti, S. Tacchi, G. Carlotti, G. Gubbiotti, G. Consolo, F. Mancoff, M.A. Yar, and J. Åkerman, Nat. Nanotech. 6, 635 (2011) DOI: 10.1038/NNANO.2011.140.
[82] L. Giovannini, F. Montoncello, and F. Nizzoli, Phys. Rev. B 75, 024416 (2007).
[83] R. Zivieri, F. Montoncello, L. Giovannini, F. Nizzoli, S. Tacchi, M. Madami, G. Gubbiotti, G. Carlotti, and A. O. Adeyeye, Phys. Rev. B 83, 054431 (2011).
[84] R. Zivieri, F. Montoncello, L. Giovannini, F. Nizzoli, S. Tacchi, M. Madami, G. Gubbiotti, G. Carlotti, and A. O. Adeyeye, IEEE Trans. Magn. 47, 1563 (2011).
[85] J. O. Vasseur, L. Dobrzynski, B. Djafari-Rouhani, and H. Puszkarski, Phys. Rev. B 54, 1043 (1996).
[86] H. Puszkarski and M. Krawczyk, Solid State Phenom. 94, 125 (2003).
[87] A. Y. Galkin, B. A. Ivanov, and C. E. Zaspel, Phys. Rev. B 74, 144419 (2006).
[88] R. Antos, Y. Otani, and J. Shibata, J. Phys. Soc. Jap. 77, 031004 (2008), and references therein.

[89] M. J. Pechan, C. T. Yu, R. L. Compton, J. P. Park, and P. A. Crowell, J. Appl. Phys. 97, 10J903 (2005).
[90] S. Neusser, B. Botters, and D. Grundler, Phys. Rev. B 78, 054406 (2008).
[91] S. Neusser, B. Botters, M. Becherer, D. Schmitt-Landsiedel, and D. Grundler, Appl. Phys. Lett. 93, 122501 (2008).
[92] V. V. Kruglyak, A Barman, R. J. Hicken, J. R. Childress, and J. A. Katine, Phys. Rev. B 71, 220409 (2005).
[93] S. Tacchi, F. Montoncello, M. Madami, G. Gubbiotti, G. Carlotti, L. Giovannini, R. Zivieri, F. Nizzoli, S. Jain, A. O. Adeyeye, and N. Singh, Phys. Rev. Lett. 107, 127204 (2011).
[94] R. Huber and D. Grundler, Proc. SPIE 8100, 81000D (2011).
[95] R. D. McMichael and M. D. Stiles, J. Appl. Phys. 97, 10J901 (2005).
[96] F. Montoncello, L. Giovannini, F. Nizzoli, P. Vavassori, M. Grimsditch, T. Ono, G. Gubbiotti, S. Tacchi, and G. Carlotti, Phys. Rev. B 76, 024426 (2007).
[97] F. Montoncello, L. Giovannini, F. Nizzoli, R. Zivieri, G. Consolo, and G. Gubbiotti, J. Magn. Magn. Mater. 322, 2330 (2010).
[98] K. Y. Guslienko and A. N. Slavin, J. Appl. Phys. 87, 6337 (2000).
[99] R. Zivieri and R. L. Stamps, Phys. Rev. B 73, 144422 (2006).
[100] M. Donahue and D. Porter, OOMMF: Object Oriented MicroMagnetic Framework, Interagency report NISTIR 6376, National Institute of Standards and Technology, Gaithersburg, MD. http://math.nist.gov/oommf.
[101] M. Slodička and L. Baňas, Appl. Math. Comp. 158, 79 (2004).
[102] M. Grimsditch, L. Giovannini, F. Montoncello, F. Nizzoli, G. K. Leaf, and H. G. Kaper, Phys. Rev. B 70, 054409 (2004).
[103] R. P. Tiwari and D. Stroud, Phys. Rev. B 81, 220403(R) (2010).
[104] M. L. Sokolovskyy and M. Krawczyk, Journal of Nanoparticle Research 13, 6085 (2011), DOI: 10.1007/s11051-011-0303-5.
[105] J. W. Klos, M. Krawczyk, and M. L. Sokolvskyy, J. Appl. Phys. 109, 07D311 (2011).
[106] S. Neusser, G. Duerr, S. Tacchi, M. Sokolovskyy, M. Madami, G. Gubbiotti, M. Krawczyk, and D. Grundler, Phys. Rev. B 84, 094454 (2011).
[107] S. Mamica and M. Krawczyk, *Tuning of the spin-wave band structure in 2D magnetic composites*, Proceedings of ICCM-18, August 21-26, 2011, Jeju Island, Korea (in press).
[108] S. Neusser, H.G. Bauer, G. Duerr, R. Huber, S. Mamica, G. Woltersdorf, M. Krawczyk, C.H. Back, and D. Grundler. Phys. Rev. B 84, 184411 (2011).
[109] P. Chu, D. L. Mills, and R. Arias, Phys. Rev. B 73, 094405 (2006).
[110] E. Tartakovskaya, W. Kreuzpaintner, and A. Schreyer, J. Appl. Phys. 103, 023913 (2008).
[111] M. Krawczyk and H. Puszkarski, Cryst. Res. Techn. 41, 547 (2006).
[112] M. Krawczyk and H. Puszkarski, Phys. Rev. B 777, 054437 (2008).
[113] M. Krawczyk, J. Klos, M. L. Sokolovskyy, and S. Mamica, J. Appl. Phys. 108, 093909 (2010).
[114] S. - K. Kim, J. Phys. D: Appl. Phys. 43, 264004 (2010), and references therein.
[115] M. Dvornik and V. V. Kruglyak, Phys. Rev. B 84, 140405 (2011).
[116] F. Giesen, J. Podbielski, T. Korn, M. Steiner, A. van Staa, and D. Grundler, Appl. Phys. Lett. 86, 112510 (2005).

[117] J. Topp, D. Heitmann, M. Kostylev, and D. Grundler, Phys. Rev. Lett. 104, 207205 (2010).
[118] J. Topp, G. Duerr, K. Thurner, and D. Grundler, Pure Appl. Chem. 83, 1989 (2011).
[119] V. V. Kruglyak, P. S. Keatley, A. Neudert, M. Delchini, R. J. Hicken, J. R. Childress, and J. A. Katine, Phys. Rev. B 77, 172407 (2008).
[120] E. J. Kim, J. L. R. Watts, B. Harteneck, A. Scholl, A. Young, A. Doran, and Y. Suzuki, J. Appl. Phys. 109, 07D712 (2011).
[121] V. L. Zhang, Z. K. Wang, H. S. Lim, S. C. Ng, M. H. Kuok, S. Jain, and A. O. Adeyeye, J. Nanosci. Nanotechn. 11, 2657 (2011).
[122] P. Rovillain, R. de Sousa, Y. Gallais, A. Sacuto, M. A. Measson, D. Colson, A. Forget, M. Bibes, M. Barthelemy, and M. Cazayous, Nature Mater. 9, 975 (2010).
[123] A. Kumar, J. F. Scott, and R. S. Katiyar, Appl. Phys. Lett. 99, 062504 (2011).
[124] T. Fischbacher, M. Franchin, G. Bordignon, and H. Fangohr. IEEE Trans. Magn. 43, 2896 (2007), http://nmag.soton.ac.uk.
[125] M. Donahue, and D.G. Porter, OOMMF User's guide, Version 1.0, Interagency Report NISTIR 6376, NIST, 1999, http://math.nist.gov/oommf.
[126] D. V. Berkov, and N. L. Gorn, MicroMagus – package for micromagnetic simulations, http://www.micromagus.de.
[127] O. Kasyutich, A. Sarua, and W. Schwarzacher, J. Phys, D – Appl. Phys. 41, 134022 (2008).
[128] O. Kasyutich, D. Tatchev, A. Hoell, F. Ogrin, C. Dewhurst, and W. Schwarzacher, J. Appl. Phys. 105, 07B528 (2009).
[129] D. F. Farrell, Y. Ijiri, C. V. Kelly, J. A. Borchers, J. J. Rhyne, Y. Ding, and S. A. Majetich, J. Magn. Magn. Mater. 303, 318 (2006).
[130] F. C. Meldrum, V. J. Wade, D. L. Nimmo, B. R. Heywood, and S. Mann, Nature 349, 684 (1991).
[131] J. Podbielski, F. Giesen, M. Berginski, N. Hoyer, and D. Grundler, Superlattices and Microstructures 37, 341 (2005).
[132] S. Neusser, G. Duerr, H. G. Bauer, S. Tacchi, M. Madami, G. Woltersdorf, G. Gubbiotti, C. H. Back, and D. Grundler, Phys. Rev. Lett. 105, 067208 (2010).
[133] H. Li, M. T. Klem, K. B. Sebby, D. J. Singel, M. Young, T. Douglas, and Y. U. Idzerda, J. Magn. Magn. Mater. 321, 175.
[134] N. Guskos, E.A. Anagnostakis, and A. Guskos, JAMME 24, 26 (2007).
[135] K. J. Kennewell, M. Kostylev, and R. L. Stamps, J. Appl. Phys. 101, 09D107 (2007).
[136] T. Suntola and J. Antson, "Method for producing compound thin films", US Patent 4058430 (1974).
[137] B. S. Lim, A. Rahtu, and R. G. Gordon, Nature Mater. 2, 749 (2003).
[138] M. Daub, M. Knez, U. U. Gösele, and K. Nielsch, J. Appl. Phys. 101, 09J111 (2007).
[139] J. Bachmann, J. Jing, M. Knez, S. Barth, H. Shen, S. Mathur, U. Gösele, and K. Nielsch, J. Am. Chem. Soc. 129, 9554 (2007).
[140] A. F. I. Morral, D. Spirkoska, J. Arbiol, M. Heigoldt, J. R. Morante, and G. Abstreiter, Small 4, 899 (2008).
[141] I. Kazeminezhad and W. Schwarzacher, Electrochem. Solid-State. Lett. 11, K24-6 (2008).
[142] P. Aranda and J. M. García, J. Magn. Magn. Mater. 249, 214 (2002), and references therein.
[143] P. R. Evans, G. Yi, and W. Schwarzacher, Appl. Phys. Lett. 76, 481 (2000).

[144] A. Robinson and W. Schwarzacher, J. Appl. Phys. 93, 7250 (2003).
[145] A. Saib, D. Vanhoenacker-Janvier, I. Huynen, A. Encinas, L. Piraux, E. Ferain, and R. Legras, Appl. Phys. Lett. 83, 2378 (2003).

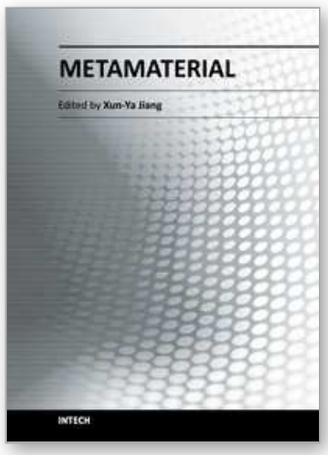

Metamaterial

Edited by Dr. Xun-Ya Jiang

ISBN 978-953-51-0591-6
Hard cover, 620 pages
Publisher InTech
Published online 16, May, 2012
Published in print edition May, 2012

In-depth analysis of the theory, properties and description of the most potential technological applications of metamaterials for the realization of novel devices such as subwavelength lenses, invisibility cloaks, dipole and reflector antennas, high frequency telecommunications, new designs of bandpass filters, absorbers and concentrators of EM waves etc. In order to create a new devices it is necessary to know the main electrodynamical characteristics of metamaterial structures on the basis of which the device is supposed to be created. The electromagnetic wave scattering surfaces built with metamaterials are primarily based on the ability of metamaterials to control the surrounded electromagnetic fields by varying their permeability and permittivity characteristics. The book covers some solutions for microwave wavelength scales as well as exploitation of nanoscale EM wavelength such as visible specter using recent advances of nanotechnology, for instance in the field of nanowires, nanopolymers, carbon nanotubes and graphene. Metamaterial is suitable for scholars from extremely large scientific domain and therefore given to engineers, scientists, graduates and other interested professionals from photonics to nanoscience and from material science to antenna engineering as a comprehensive reference on this artificial materials of tomorrow.

How to reference

In order to correctly reference this scholarly work, feel free to copy and paste the following:

V.V. Kruglyak, M. Dvornik, R.V. Mikhaylovskiy, O. Dmytriiev, G. Gubbiotti, S. Tacchi, M. Madami, G. Carlotti, F. Montoncello, L. Giovannini, R. Zivieri, J.W. Klos, M.L. Sokolovskyy, S. Mamica, M. Krawczyk, M. Okuda, J.C. Eloi, S. Ward Jones, W. Schwarzacher, T. Schwarze, F. Brandl, D. Grundler, D.V. Berkov, E. Semenova and N. Gorn (2012). Magnonic Metamaterials, Metamaterial, Dr. Xun-Ya Jiang (Ed.), ISBN: 978-953-51-0591-6, InTech, Available from: http://www.intechopen.com/books/metamaterial/magnonic-metamaterials

INTECH
open science | open minds

InTech Europe
University Campus STeP Ri
Slavka Krautzeka 83/A
51000 Rijeka, Croatia
Phone: +385 (51) 770 447
Fax: +385 (51) 686 166
www.intechopen.com

InTech China
Unit 405, Office Block, Hotel Equatorial Shanghai
No.65, Yan An Road (West), Shanghai, 200040, China
中国上海市延安西路65号上海国际贵都大饭店办公楼405单元
Phone: +86-21-62489820
Fax: +86-21-62489821

IntechOpen